Mathematical Modelling of Engineering Problems
Vol. 12, No. 2, February, 2025, pp. 687-708
Journal homepage: http://iieta.org/journals/mmep

Impact of Porosity Distribution on Vibration of Porous Functionally Graded Beams

Nadia Kareem Abood[1,2*], Luay S. Al-Ansari[2]

[1] Vocational Education Department, Najaf Al-Ashraf Education Directorate, Najaf 54001, Iraq
[2] Department of Mechanical Engineering, University of Kufa, Najaf 54001, Iraq

Corresponding Author Email: nadiak.alzobaie@student.uokufa.edu.iq

https://doi.org/10.18280/mmep.120232

Received: 19 February 2024
Revised: 8 May 2024
Accepted: 15 May 2024
Available online: 28 February 2025

Keywords:
porous beam, natural frequency, functionally graded beam, power law model, ANSYS software, finite element method

ABSTRACT

In this work, the free vibration investigation of a porous-functionally-graded-beam (FGB) along its height utilizing first-order-shear-deformation theory (FOSDT) with different supporting types, including clamped-clamped, clamped-free and simply supported, is studied. The power-law equation is used to describe distribution of mechanical properties of functionally-graded-beam (FGB). The materials used in a typical case of functionally-graded-beam (FGB) consists of aluminum and alumina (Al_2O_3). Three types of porosity distribution functions: even uniform distribution, uneven-I central distribution and uneven-II corner distribution are considered. The finite element model is applied by utilizing the ANSYS APDL 17.2 and using element "SHELL28" to calculate the natural frequencies and show the impacts of length/height ratio, index of power-law model K, distribution of porosity and porosity index (α-index). The present model's results were compared to literature, showing good agreement. For even porous functionally-graded-beam (PFGB), as the power-law-index K rises, the first three frequency parameters decrease, while increasing the porosity index decreases the frequency parameter. The influence of power-law-index and porosity index is observed in Uneven-I and Uneven-II porous-FGBs. The length/height ratio has minimal influence. Frequency parameters increase with higher mode numbers. Uneven-I materials causes the smallest influence of porosity on the frequency parameters due to distribute the porosity near the center of cross section area of beam.

1. INTRODUCTION

Composite materials are one of the modern materials created to develop the material properties to achieve the requirement of the modern engineering applications. The physical combination of two or more materials is the basic idea of composite material. Several methods can be used to achieve this combination and to get better material properties, and one of these methods is the combination of different materials as layered media, called laminated composite materials and this type of combination leads to the occurrence of stress and temperature discontinuities in the material [1]. In 1980, functionally-graded-material (FGM) is a novel type of materials. FGM was suggested to overcome this problem. The properties of these materials undergo a progressive transformation from the first material to second one based on a specified equation. Nowadays, because of their higher material properties, FG materials are applied in different fields, especially in nuclear, biomedical, aerospace, and optical engineering applications [2-5]. Numerous studies on the mechanical behavior of structures have been done as a result of the widespread uses of FGM [6-13]. However, during the manufacturing process, these materials may display certain flaws like porosity. Therefore, a study on this topic has to be added as soon as possible to have a solid understanding of the porosity influence on the mechanical and structural behaviors of FGM. Because of its various applications, beams—along with plates and shells—have always piqued the interest of researchers among the three types of structures. Simple beam theories such as classical, first, second and higher-order-shear-deformation theory are just a few of the many beam theories that are used to analyze beam structures. On the other hand, researchers can lower the computational cost and keep the resulting error within the permitted range by employing a straightforward model. Furthermore, in order to give the designer an accurate understanding of the mechanical properties, beams composed of FGM with porosity must be thoroughly investigated.

Chen et al. [14] investigated the static bending and elastic buckling of porous-FGB depending on Timoshenko-beam-theory (TBT). The mechanical properties and porosity are gradually distribution along the height of FGB. Two distribution models are used to describe the porosity distribution. They calculated the transverse displacement and critical buckling using Ritz method with various supporting type, i.e., boundary conditions (BC) to investigate the impact of length/height ratio and porosity. Also, Wattanasakulpong and Chaikittiratana [15] analyzed the transverse beam vibration under various boundary conditions considering the impact of inertia and shear effect and using TBT. To determine the material parameters of the FGBs, such as the volume fraction, the revised rule of mixture was utilized of porosity assuming three types of porous distribution models across the beam section. They calculated the natural frequencies of porous-FGBs under various supported ends and they found that "FGM beams with uniform porosity distribution have a stronger influence on natural frequencies compared to uneven porous-FGBs. This method is effective for eigenvalue analysis of structural problems".

In 2016, Al Rjoub and Hamad [16] improved new analytical solution to investigate free vibration of porous-FGB with different boundary conditions using Euler-Bernoulli-theory (EBT) and Timoshenko-beam-theory (TBT). They employed the transfer-matrix method in order to compute non-dimensional frequencies of pure and porous FGBs assuming uniform distribution of porosities along the height of the beam. Their results showed the effects of material index, volume fraction, boundary conditions, length/height ratio, and porosity on dimensionless frequency parameters of pure and porous FGBs. Galeban et al. [17] investigated the free vibration of porous beams by deriving the governing equations using Euler-Bernoulli theory. The mechanical properties are changes in the cross-section porous beam. The results showed that the porosity, mass, fluid compressibility, distribution of pores and supporting types, i.e., boundary conditions (BC) impact the natural frequencies of beams. Hinged-hinged beams exhibit unique natural frequency behavior.

Fouda et al. [18] investigated the porosity influence on the mechanical behavior of FGB assuming Euler-Bernoulli theory and power distribution along the thickness of FG beam to construct the governing equations and the kinematic relations. They concluded that “the static deflection and buckling load affected the porosity and the material distribution parameter, while the frequency is influenced by the material index and has a stronger correlation with porosity in the proposed model”. Akbaş [19] studied the forced vibrations of porous FGBs subjected to dynamic loading. In deep beam, the mechanical properties vary across the height of FGB due to the presence of porosity. The finite element method is utilized to resolve the problems within the "plane solid continua model". Amir et al. [20] analyzed the vibration of a sandwich micro-beam composed of a porous core and face sheets reinforced with FG carbon nanotubes and supported on a Winkler-Pasternak substrate. They considered in their analysis the beam's response to thermal load and employed "sinusoidal-shear-deformation-beam-theory" (SSDBT) to define the displacement components assuming that the properties of the core and facial sheets are dispersed throughout its height. They applied "Hamilton’s principle" and "Navier’s method" to drive the equations of motion to study the influence of porosity value and function, small scale, various kinds of CNTs distribution, and geometrical beam size. The study findings indicate that the frequency decreases when the porosity increases.

In 2020, Zanoosi [21] studied the vibration of a porous-FG micro-beam while considering the influence of thermal effects by utilizing the elasticity of modified strain gradient theory (MSGT). They used MSGT instead of MCST to analyze the size-dependent porous structures and they applied "Hamilton's principle" and the "Navier solution" to determine the natural frequency the micro-beam under simply supported conditions. They investigated the influence of temperature changes, length scale, material index, length/height ratio, and volume fraction of porosity on FG micro-beam natural frequency. They concluded that the temperature increases reduced the micro-beam's frequency. Zghal et al. [22] used a "refined-mixed-finite-element-beam" model for studying static bending analysis of porous-FGBs. They used two distributions of porosity, even and uneven and to ascertain the mechanical properties of porous-FGB, use a modified power-law model. They conducted a parametric study to examine how the boundary conditions, porosity coefficient, types of porosity distributions and power law index affect the displacement and stress of the FGBs. They concluded that “the porosity parameter in modern structural design of cannot be overstated. The percentage of porosity present in the structure can have a profound impact on its overall performance and response”. Rahmani et al. [23] used various theories in order to investigate bending, buckling, and study of vibration of porous-FGBs. They employed the finite element approach to solve problems assuming a power law model to represent the mechanical properties along the height of the FGB, and they used "Hamilton's principle" to drive the equation of motion. They investigated the impact of porosity exponents, power-law index, and supporting type on the bending behavior, buckling characteristics, and natural frequencies of the beam using ANSYS Software. They found that the displacement, critical buckling and frequencies increase when length /height ratio increases. Also, the nondimensional frequencies decrease with decreasing values of the porosity index and power-law index. Ultimately, the FG beam becomes less rigid as porosity and power-law index increase, leading to higher deflection and decreased critical buckling load”. Karamanli and Vo [24], used three alternative models of porosity distribution to examine the size-dependent behavior of porous-FG micro-beams using a quasi-3D theory and a modified-strain-gradient-theory (MSGT). They applied the rule of mixture for determining material properties and material length scale parameters (MLSPs) based on the porosity index, thickness, and material index, thereby enabling a comprehensive understanding of the material characteristics. They checked the accuracy of the suggested model and studied the impacts of varying MLSP, material index, porosity index, and boundary condition on responses of porous-FG micro-beam.

Rahmani [25] modified the "high-order-sandwich-beam-theory" to investigate the frequency responses of clamped-free sandwich beams with homogeneous face sheets and a FG core using a modified power-law model and two porosity distribution models to characterize the material qualities along its height. They used "Hamilton’s principle" and a "Galerkin method" to solve Governing equations of motion. They showed a comparison with specific scenarios outlined in existing literature. They concluded that “as a power-law index, temperature, cross-section, length, and porosity volume fraction increase, the basic frequency parameter falls. Conversely, an increase in the wave number leads to an increase in the frequency”. Anirudh et al. [26] used a "trigonometric-shear-deformation-theory" to examine the transverse vibration and buckling behavior of curved beams composed of porous-FG graphene-reinforced nanocomposites to study the impact of various theories on the static and dynamic performance. They used Lagrangian equations of motion and finite element analysis to derive the equilibrium equations. They conducted a comprehensive study to assess how parameters such as radius of curvature, porosity coefficient, length-to-thickness ratio, distribution pattern of porosity and graphene platelets, platelet geometry, and supporting types affect static bending, elastic stability and free vibration.

Ton [5] studied the impact of porosity on the free vibration behavior of a porous FGB using simple beam theory. He examined the effects of boundary conditions, porosity distribution models, and material distribution on the free vibration problem of porous FGB. He concluded that "the results align well with existing references and confirm the applicability of classical beam theory in analyzing functionally graded porous beams. The mechanical information provided may prove useful to designers for specific purposes". Adıyaman [1] analyzes the porous-FGB's free vibration behavior utilizing a higher-order-shear-deformation-theory (HOSDT). He used Lagrange's principle, power law model, and different porosity distribution functions to derive the governing equations and applied FEM to solve these equations. He calculated the dimensionless natural frequencies and studied the influence of material properties, supporting types, and porosity on the nondimensional frequency and mode shape. His results showed that "The mode shapes have comparable traits. despite the influence of porosity on frequencies". Nguyen et al. [27] investigated three models of porosity distribution using a straightforward two-variable shear-deformation-theory (SDT) to analyze the transverse displacement, bucking, and vibration problems of porous-FGBs. They used Lagrange's principle, the power law model to derive the governing equations. They applied exponential approximations to determine the buckling. load, displacement., frequency, and. stress of beams under various supporting types using ANSYS model. They studied the influence of boundary conditions, porosity parameters, porous distribution pattern, height-to-span ratio, and shear deformation on the stress., deflection., frequency., and critical buckling load of beams. Turan et al. [28], analyzed the. buckling behavior and porous-FGB's unrestricted vibration under different boundary conditions considering first-order-shear-deformation-theory (FOSDT). They used the power law model, Lagrange's principle, and the Ritz method to derive and solve the equations of motion analytically. While they used Finite-Element-Method (FEM) and artificial-neural-network-method (ANN) to solve the problem numerically. They investigated the critical buckling loads and normalized natural frequencies for different boundary conditions, porosity coefficient, power-law index, length/height ratio, and porosity distribution models. Their results obtained from the analytical, FEM, and ANN methods were found to be in good agreement.

In this paper, the Finite-Element-Model is built using ANSYS software to calculate the free vibration behavior of porous-FGB and study the impacts of porosity and material distribution and supporting types on the natural frequencies and shape mode, in addition to length/height ratio important parameters, which is don't study previously.

In order to achieve these points, this paper is divided into: **Problem Description**: in this part, the configuration of the porous-FGB and the variation of mechanical properties due to materials and porosity distributions are described. In the next part, **ANSYS or Finite element Model** is described in detail, and the third part **Validation of the ANSYS Model** deals with the comparison between the frequency results of the ANSYS model and that of available literature. Finally, the part **Results and Discussion** is used to describe the frequency results due to variation of length/height ratio, power-law index K, porosity distribution, and porosity index (α-index).

2. PROBLEM DESCRIPTION

Changes in the FG's mechanical and physical characteristics beam along its height are necessary for a number of structural and mechanical applications. Three widely used models were used to characterize this difference in material properties over the height of the FGB: The sigmoid, exponential, and power-law models. A FGB with dimensions of length (L), height (h), and width (W) is examined in this work as illustrated in Figure 1. The variation of elastic modulus, density, and Poisson ratio along the height of FGB can described as following equations using the power-law model [29, 30]:

$$E(z) = \left(E_{top} - E_{bottom}\right)\left(0.5 + \frac{z}{h}\right)^k + E_{bottom} \tag{1a}$$

$$\mu(z) = \left(\mu_{top} - \mu_{bottom}\right)\left(0.5 + \frac{z}{h}\right)^k + \mu_{bottom} \tag{1b}$$

$$\rho(z) = \left(\rho_{top} - \rho_{bottom}\right)\left(0.5 + \frac{z}{h}\right)^k + \rho_{bottom} \tag{1c}$$

where, $E(z)$, $\mu(z)$ and $\rho(z)$ are the elastic modulus of, Poisson ratio and density at any point in height of FGB. E_{top} and E_{bottom} are the elastic modulus of top and bottom materials. μ_{top} and μ_{bottom} are Poisson ratio of top and bottom materials. ρ_{top} and ρ_{bottom} are the density of top and bottom materials. k is power-law index or material distribution index.

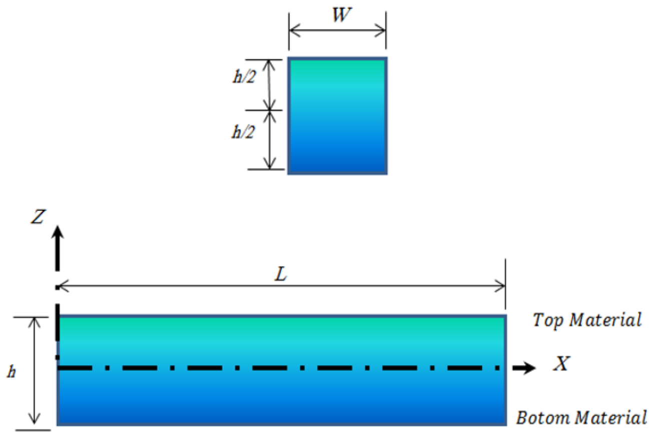

Figure 1. The geometry of FG beam

Two types of materials that are frequently utilized in the creation of FGMs are ceramics and metal. But during the fabrication process, voids and cavities, which are typically created in contrast to the metallic phase, in the ceramic phase form in the FG materials. Researchers have been concentrating on figuring out how this porosity affects the FG beam's mechanical behavior lately. Several researchers assumed the material qualities are generally impacted by the porosity in the beam and can described as:

$$E(z) = \left(E_{top} - E_{bottom}\right)\left(0.5 + \frac{z}{h}\right)^k + E_{bottom} - \left(\frac{\alpha}{2}\right) * g(z) * \left(E_{top} + E_{bottom}\right) \tag{2a}$$

$$\mu(z) = \left(\mu_{top} - \mu_{bottom}\right)\left(0.5 + \frac{z}{h}\right)^k + \mu_{bottom} - \left(\frac{\alpha}{2}\right) * g(z) * \left(\mu_{top} + \mu_{bottom}\right) \tag{2b}$$

$$\rho(z) = \left(\rho_{top} - \rho_{bottom}\right)\left(0.5 + \frac{z}{h}\right)^k + \rho_{bottom} - \tag{2c}$$

$$\left(\frac{\alpha}{2}\right) * g(z) * \left(\rho_{top} + \rho_{bottom}\right)$$

where, α-index is the porosity index (0<α-index<1) and $g(z)$is the function described the porosity distribution in the cross-section area of porous beam. In this work, even, uneven-I and uneven-II porosity distributions are considered as shown in Figure 2 and these porosity distributions can be described by the following equations:

$$g_1(z) = 1 \tag{3a}$$

$$g_2(z) = 1 - \frac{2|z|}{h} \tag{3b}$$

$$g_3(z) = Sin\left(\frac{\pi|z|}{h}\right) \tag{3c}$$

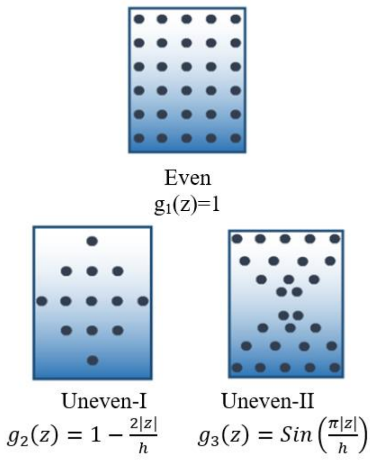

Figure 2. The functions of porosity distribution used in this work [1]

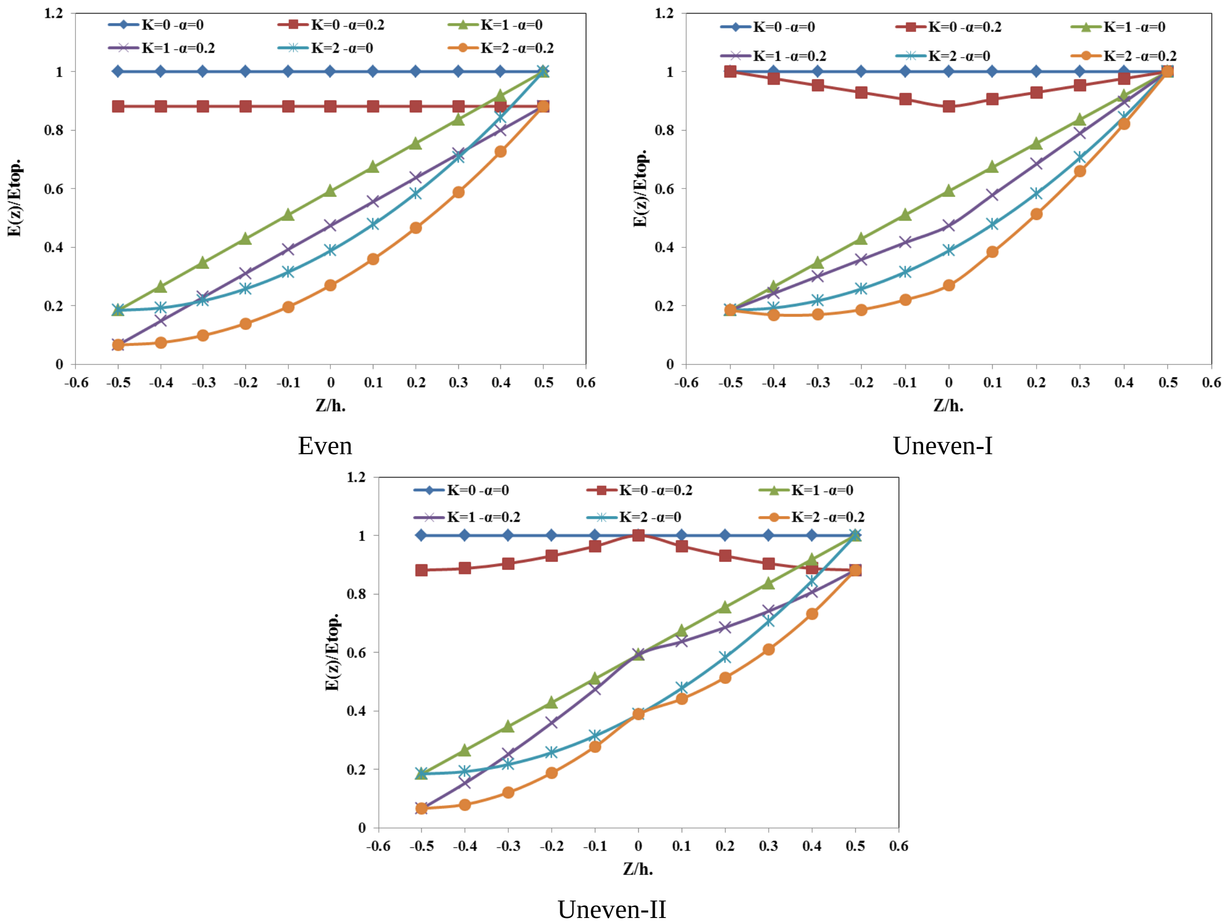

Figure 3. Young's modulus ratio (E(z)/Etop) in Even, Uneven-I and Uneven-II when K=0, 1 and 2, and α-index=0 and 0.2

3. ANSYS MODEL

The ANSYS model used the element "SHELL281" for simulating the variation of the properties across the height of FGB. The characteristics of "SHELL281" are: "Analysis of thin to moderately-thick shell structures are appropriate for SHELL281. The element consists of eight nodes, each of which has six degrees of freedom: x, y, and z axis translations as well as rotations around those axes. The element only has translational degrees of freedom when the membrane option is used. Applications requiring large rotation, large strain, or both are ideally suited for SHELL281. Nonlinear analyses take into consideration changes in shell thickness. The element takes into consideration the impact of scattered stresses on followers, load stiffness. Layered applications such as sandwich building or composite shell modeling can make use of SHELL281. First-order shear-deformation theory (also known as Mindlin-Reissner shell theory controls modeling accuracy for composite shells. True stress measures and logarithmic strain serve as the foundation for the element formulation. Finite membrane strains are possible due to the element's kinematics stretching. On the other hand, it is believed that the curvature variations within a time increment are minimal" [31] (see Figure 4).

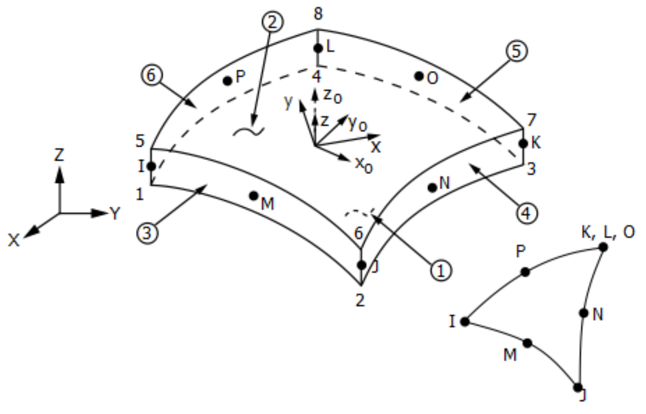

Figure 4. Geometry of SHELL281 [31]

The ANSYS model of porous-FGB was built by applying the following steps [29, 30]:

1. The FGB is drawn as the top area (L*W) as illustrated in Figure 5(a).

2. The required properties of porous-FGB are estimated by the following points:

(a) The height of beam is divided into (N) parts (in this work N=10). Each part is called "layer".

(b) The height of each layer is calculated as (height of layer= height of beam/N).

(c) From step (a), the required material properties are calculated for N+1 points along the height of porous-FGB using Eq. (2) and assuming [z_i=zo+((h/N) *(i-1))] where zo=-h/2 and (i) is number of point (1≤i≤(N+1)).

(d) The following formula is used to determine the necessary material qualities for each layer:

$$\left(E_{layer}\right)_i = \frac{E(z_i)+E(z_{i+1})}{2} \tag{4a}$$

$$\left(\mu_{layer}\right)_i = \frac{\mu(z_i)+\mu(z_{i+1})}{2} \tag{4b}$$

$$\left(\rho_{layer}\right)_i = \frac{\rho(z_i)+\rho(z_{i+1})}{2} \tag{4c}$$

3. The (N) set of material properties are input into the ANSYS APDL software using the commend "section" assuming the layer is isotropic material as shown in Figure 5(b).

4. The drawing area is meshing using the element "SHELL281" as shown in Figure 5(c) considering the convergence criteria of element size.

5. Three types of supports are considered in this work, clamped-clamped beam (C-C), simply supported beam (S-S) and clamped-free beam (C-F). The boundary conditions of each type of supports are:

(a) Clamped-Clamped beam (C-C): All degree of freedom (UX, UY, UZ, ROTX, ROTY and ROTZ) of the nodes at edges x=0 and x=L are zero.

(b) Simply Supported beam (S-S): The degree of freedom (UX, UY and UZ) of the nodes at edge x=0 is zero. Also, the degree of freedom (UY and UZ) of the nodes at edge x=L are zero.

(c) Clamped-Free beam (C-F): All degree of freedom (UX, UY, UZ, ROTX, ROTY and ROTZ) of the nodes at edge x=0 only is zero.

The model analysis is selected to analyze the free vibration problem of porous-FGB as shown in Figure 5(d).

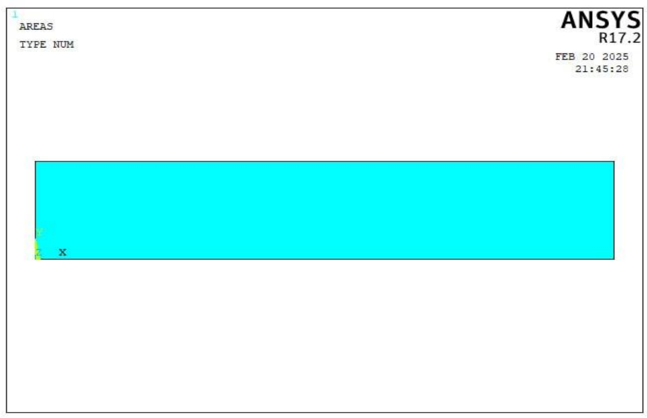

(a) Beam geometry

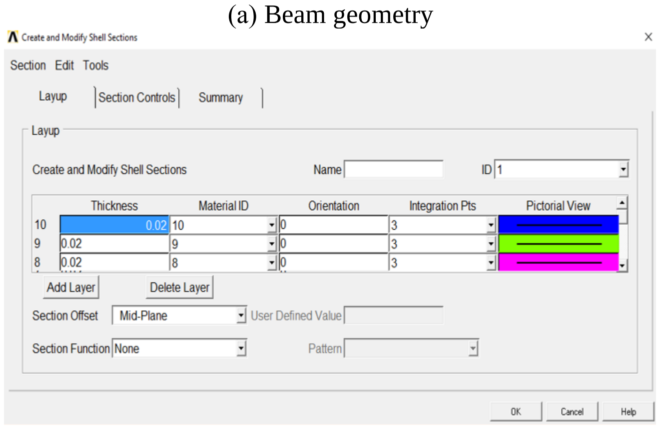

(b) Height and properties of each layer

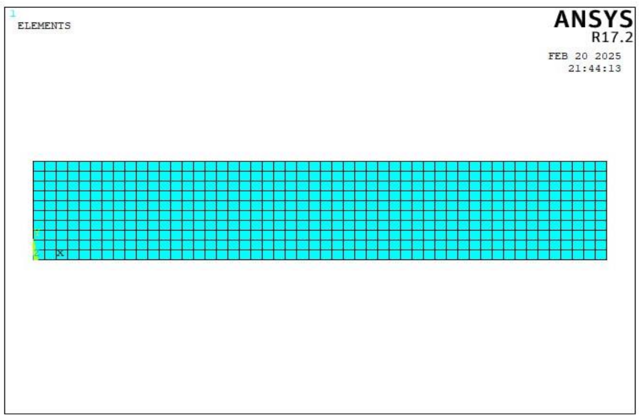

(c) Meshing of drawn area

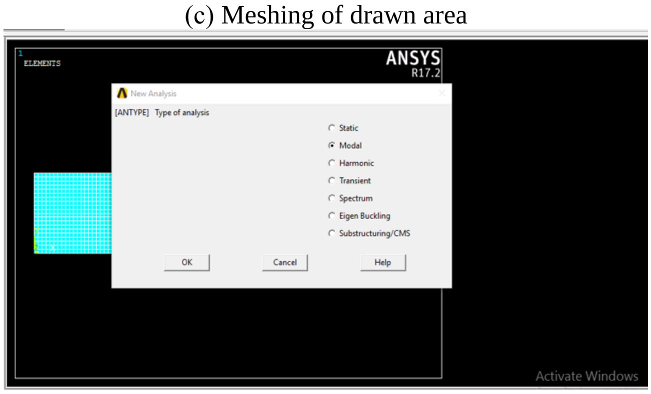

(d) Analysis type

Figure 5. General steps of present ANSYS model

4. VALIDATION OF ANSYS MODEL

To verify the ANSYS model that is employed in this paper, the comparisons between the natural frequency results of the present model and that found in available literatures ware made. In this comparison, the FGB consists of aluminum and Alumina. The material properties of these materials are listed in Table 1.

Table 1. The aluminum and alumina material properties [4]

Properties	Unit	Metal	Ceramic
Modulus of Elasticity (E)	GPa	70	380
Density (ρ)	Kg/m^3	2707	3960
Poisson Ratio (μ)	-	0.3	0.3

(a) Functionally graded beam without porosity

The first comparison is made between the frequency results of the present model with that of Kahya and Turan [32] utilizing the FEM approach based on FOSDT. Nguyen et al. [33] used HOSDT as the foundation for an analytical solution technique. Vo et al. [34] implemented FEM with an advanced theory of shear deformation and Gökhan Adıyaman [1] employed FEM with HOSDT as a basis for the perfect cross section of power law FG beam, i.e., non-pours FG beam (see Table 2). Where the equation can be used to compute the dimensionless frequency parameter:

$$\bar{\omega} = \frac{\omega L^2}{h} \sqrt{\frac{\rho_m}{E_m}} \tag{5}$$

There is a great deal of agreement in the comparison. with the results of present model and that of available literatures for FGB with different material index and various supporting types (S-S, C-C and C-F).

(b) Functionally graded beam with porosity

The second comparison is mode to validate the authenticity of the current model of the porous-FGB. Three parameters were studied, and theses parameters were power law index 0, 0.5, 1, 2, 5 and 10, porosity index 0, 0.1, 0.2 and 0.3 and supporting type S-S, C-C and C-F in additional to the distribution function of porosity, Even, Uneven-I and Uneven-II. Tables 3-5 show the dimensionless frequency comparison between of the porous-FGB obtained by present model and that of Adıyaman [1] when the distribution function of porosity is Even, Uneven-I and Uneven-II respectively.

For different distribution of porosity, Even, Uneven-I, Uneven-II, the porous-FGB's frequency parameter results are closely matched for different porosity index, boundary conditions and the power law index and the maximum discrepancy between the comparing results is not exceed 10% (see Figures 6-8). From Figure 6, the maximum discrepancy between the comparing results is approximately 4.5% for each supporting type and Even distribution function of porosity. While the maximum discrepancy between the comparing results is 3.5%, 10% and 9.5% for S-S, C-C and C-F supports respectively and when the distribution function of porosity is Uneven-I (see Figure 7). For Uneven-II, the maximum discrepancy between the comparing results is 0.75%, 0.5% and 4.5% for S-S, C-C and C-F supports respectively as illustrated in Figure 8.

Table 2. The comparison among the frequency results of the current work with that of Kahya and Turan [32], Nguyen et al. [33], Vo et al. [34], and Adıyaman [1] when *L*/*h*=5

B.C	References	K=0	K=0.5	K=1	K=2	K=5	K=10
SS	Kahya and Turan [32]	5.2219	4.4692	4.0496	3.6936	3.4881	3.3643
	Nguyen et al. [33]	5.1528	4.4102	3.9904	3.6264	3.4009	3.2815
	Vo et al. [34]	5.1528	4.4019	3.9716	3.5979	3.3743	3.2653
	Adıyaman [1]	5.1532	4.4016	3.9710	3.5970	3.3725	3.2644
	Present work	5.155718	4.370045	3.980049	3.60215	3.3654	3.26865
CC	Kahya and Turan [32]	10.0864	8.7547	7.9841	7.2715	6.7148	6.3741
	Nguyen et al. [33]	10.0726	8.7463	7.9518	7.1776	6.4929	6.1658
	Vo.et al. [34]	10.0678	8.7457	7.9522	7.1801	6.4961	6.1662
	Adıyaman [1]	10.0321	8.7114	7.9200	7.1496	6.4626	6.1355
	Present work	10.0660	8.70081	7.962938	7.16084	6.4396	6.10286
CF	Kahya and Turan [32]	1.9077	1.6286	1.4739	1.3446	1.2751	1.2636
	Nguyen et al. [33]	1.8957	1.6182	1.4636	1.3328	1.2594	1.2187
	Vo et al. [34]	1.8952	1.6180	1.4633	1.3326	1.2592	1.2184
	Adıyaman [1]	1.8948	1.6176	1.4629	1.3322	1.2586	1.2178
	Present work	1.90472	1.613582	1.473539	1.340905	1.261807	1.16474

Table 3. The frequency parameters of a porous –FGB with various porosity index (α-index), power law index K and supporting type when the porosity function is Even and *L*/*h*=5

B.C	α-Index	References	K=0	K=0.5	K=1	K=2	K=5	K=10
SS	0	Present Work	5.155718	4.370045	3.980049	3.602155	3.365477	3.268657
		Adıyaman [1]	5.1532	4.4016	3.971	3.5970	3.3725	3.2644
	0.1	Present Work	5.230494	4.360659	3.897554	3.416172	3.102989	3.007281
		Adıyaman [1]	5.2223	4.3934	3.8835	3.4050	3.1083	3.0028
	0.2	Present Work	5.318299	4.344111	3.777085	3.122255	2.635685	2.527751
		Adıyaman [1]	5.3047	4.3798	3.7577	3.1023	2.6403	2.5273
	0.3	Present Work	5.423208	4.315892	3.591473	2.594932	1.477182	1.113058

		Adıyaman [1]	5.4040	4.3573	3.5658	2.5572	1.4574	1.1164
CC	0	Present Work	10.06605	8.700818	7.962938	7.16084	6.439631	6.102861
		Adıyaman [1]	10.0321	8.7114	7.9200	7.1496	6.4626	6.1355
	0.1	Present Work	10.22968	8.718108	7.85488	6.873097	5.980539	5.630864
		Adıyaman [1]	10.1621	8.7170	7.7918	6.8439	6.0019	5.6231
	0.2	Present Work	10.42048	8.728605	7.686927	6.408757	5.180417	4.741579
		Adıyaman [1]	10.3225	8.7178	7.6032	6.3561	5.2216	4.7437
	0.3	Present Work	10.64648	8.724282	7.409681	5.536144	3.220927	2.257545
		Adıyaman [1]	10.5158	8.7094	7.3061	5.4349	3.2140	2.3636
CF	0	Present Work	1.90472	1.613582	1.473539	1.340905	1.261807	1.16474
		Adıyaman [1]	1.8948	1.6176	1.4629	1.3322	1.2586	1.2178
	0.1	Present Work	1.929666	1.608086	1.441801	1.272119	1.166963	1.091014
		Adıyaman [1]	1.9203	1.6147	1.4313	1.2630	1.1649	1.1266
	0.2	Present Work	1.959552	1.600121	1.39654	1.163999	0.997405	0.961283
		Adıyaman [1]	1.9506	1.6098	1.3858	1.1533	0.9963	0.9592
	0.3	Present Work	1.995798	1.588203	1.327815	0.969866	0.565044	0.434232
		Adıyaman [1]	1.9872	1.6016	1.3162	0.9539	0.5559	0.4339

Table 4. The frequency parameters of a porous –FGB with various porosity index (α-index), power law index K and supporting type when the porosity function is Uneven-I and L/h=5

B.C	α-Index	References	K=0	K=0.5	K=1	K=2	K=5	K=10
SS	0	Present Work	5.155718	4.370045	3.980049	3.602155	3.365477	3.268657
		Adıyaman [1]	5.1532	4.4016	3.9710	3.5970	3.3725	3.2644
	0.1	Present Work	5.223887	4.410736	3.994621	3.578135	3.308423	3.212653
		Adıyaman [1]	5.2184	4.4429	3.9850	3.5737	3.3193	3.2112
	0.2	Present Work	5.297058	4.454268	4.00802	3.543433	3.219877	3.116389
		Adıyaman [1]	5.2888	4.4872	3.9978	3.5405	3.2417	3.1252
	0.3	Present Work	5.375909	4.500826	4.019443	3.493418	3.05742	2.869708
		Adıyaman [1]	5.3644	4.5345	4.0087	3.4939	3.1251	2.9710
CC	0	Present Work	10.06605	8.700818	7.962938	7.16084	6.439631	6.102861
		Adıyaman [1]	10.0321	8.7114	7.9200	7.1496	6.4626	6.1355
	0.1	Present Work	10.18831	8.773063	7.984549	7.096622	6.251301	5.895081
		Adıyaman [1]	10.1273	8.7717	7.9324	7.0887	6.2970	5.9242
	0.2	Present Work	10.31736	8.848395	8.001839	7.004001	5.947751	5.535897
		Adıyaman [1]	10.2342	8.8350	7.9412	7.0081	6.0665	5.6045
	0.3	Present Work	10.45568	8.928049	8.011718	6.868157	5.337564	4.563499
		Adıyaman [1]	10.3482	8.9015	7.9447	6.9009	5.7300	5.0676
CF	0	Present Work	1.90472	1.613582	1.473539	1.340905	1.261807	1.16474
		Adıyaman [1]	1.8948	1.6176	1.4629	1.3322	1.2586	1.2178
	0.1	Present Work	1.930037	1.629018	1.479899	1.334175	1.240998	1.130347
		Adıyaman [1]	1.9202	1.6342	1.4699	1.3264	1.2445	1.2055
	0.2	Present Work	1.944239	1.645629	1.486073	1.324172	1.211792	1.089347
		Adıyaman [1]	1.9475	1.6521	1.4767	1.3173	1.2230	1.1844
	0.3	Present Work	1.959429	1.663535	1.491878	1.309352	1.175669	1.037479
		Adıyaman [1]	1.9769	1.6713	1.4830	1.3038	1.1895	1.1455

Table 5. The frequency parameters of a porous –FGB with various porosity index (α-index), power law index K and supporting type when the porosity function is Uneven-II and L/h=5

B.C	α-Index	References	K=0	K=0.5	K=1	K=2	K=5	K=10
SS	0	Present Work	5.155718	4.370045	3.980049	3.602155	3.365477	3.268657
		Adıyaman [1]	5.1532	4.4016	3.9710	3.5970	3.3725	3.2644
	0.1	Present Work	5.169241	4.31935	3.877733	3.431423	3.151152	3.053221
		Adıyaman [1]	5.1633	4.3512	3.8633	3.4184	3.1517	3.0452
	0.2	Present Work	5.183875	4.258467	3.750719	3.206787	2.850751	2.749177
		Adıyaman [1]	5.1747	4.2911	3.7297	3.1828	2.8423	2.7376
	0.3	Present Work	5.199682	4.184309	3.589188	2.896506	2.389252	2.271006
		Adıyaman [1]	5.1872	4.2184	3.5602	2.8568	2.3646	2.2533
CC	0	Present Work	10.06605	8.700818	7.962938	7.16084	6.439631	6.102861
		Adıyaman [1]	10.0321	8.7114	7.9200	7.1496	6.4626	6.1355
	0.1	Present Work	10.12409	8.648333	7.826476	6.920642	6.142008	5.815612

		Adıyaman [1]	10.0749	8.6571	7.7698	6.8867	6.1421	5.8047
	0.2	Present Work	10.18584	8.579176	7.646174	6.585354	5.703294	5.347876
		Adıyaman [1]	10.1269	8.5875	7.5747	6.5227	5.6788	5.3373
	0.3	Present Work	10.25253	8.487173	7.401037	6.084892	4.972514	4.562697
		Adıyaman [1]	10.1832	8.4973	7.3142	5.9865	4.9161	4.5760
CF	0	Present Work	1.90472	1.613582	1.473539	1.340905	1.261807	1.16474
		Adıyaman [1]	1.8948	1.6176	1.4629	1.3322	1.2586	1.2178
	0.1	Present Work	1.906635	1.592155	1.433403	1.275577	1.180177	1.121579
		Adıyaman [1]	1.8973	1.5978	1.4222	1.2654	1.1760	1.1356
	0.2	Present Work	1.908981	1.567148	1.384375	1.190736	1.067056	1.029452
		Adıyaman [1]	1.9001	1.5743	1.3720	1.1777	1.0607	1.0209
	0.3	Present Work	1.911821	1.537385	1.322999	1.074898	0.89509	0.85217
		Adıyaman [1]	1.9032	1.5461	1.3086	1.0569	0.8832	0.8411

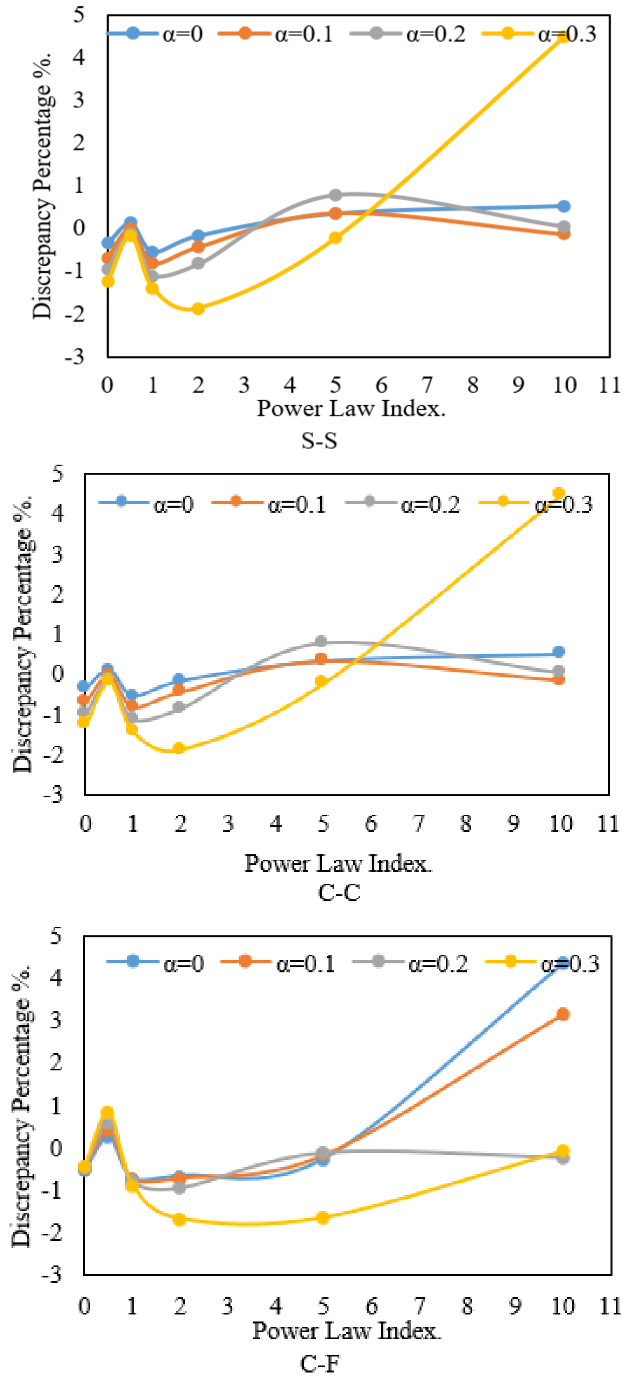

Figure 6. The discrepancy percentage of the frequency parameter of pours-FGM for various porosity index, supporting type, and power law index for Even distribution function of porosity

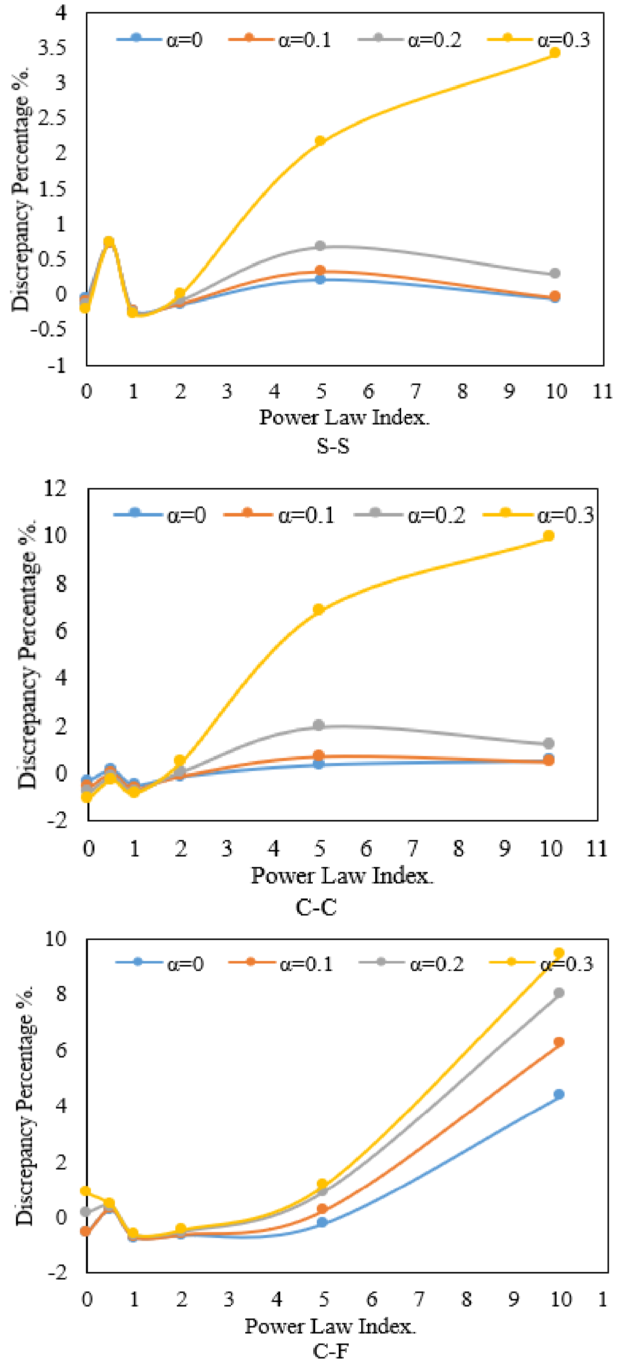

Figure 7. The discrepancy percentage of the frequency parameter of pours-FGM for various porosity index, supporting type, and power law index for Uneven-I distribution function of porosity

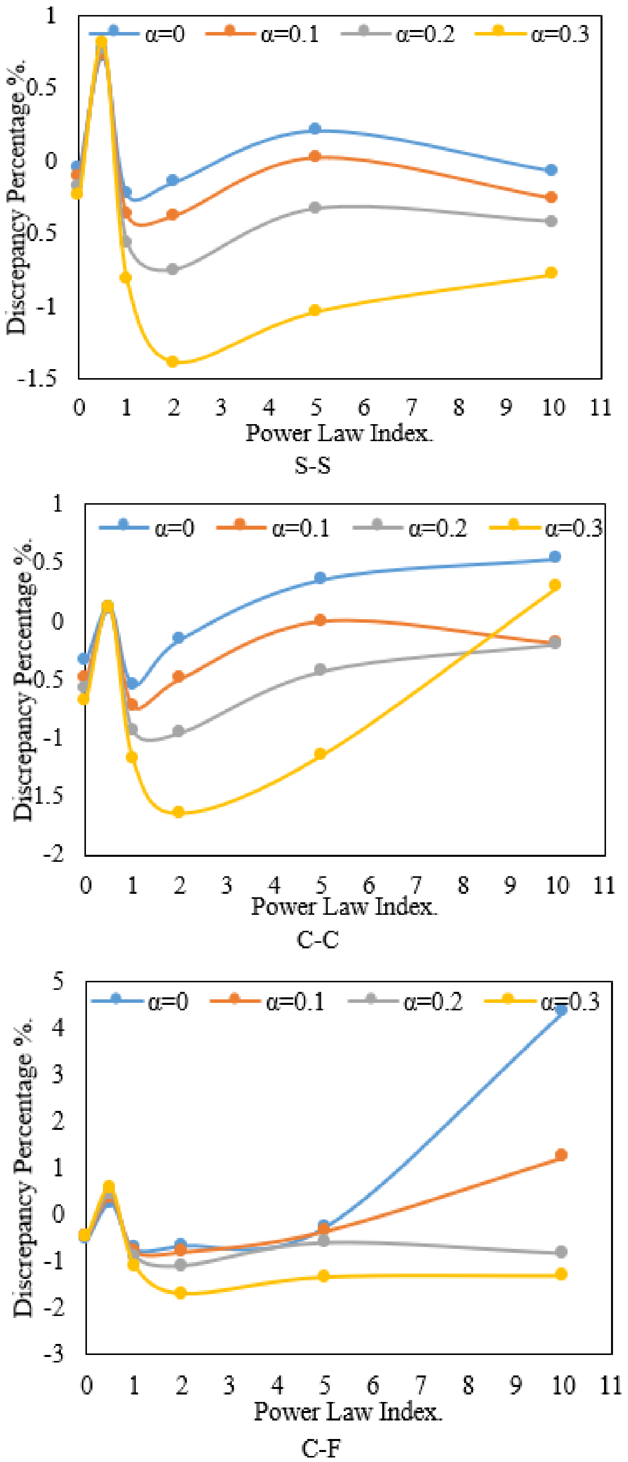

Figure 8. The discrepancy percentage of the frequency parameter of Pours-FGM for various power law index, porosity index and supporting type for Uneven-II distribution function of porosity

5. RESULTS AND DISCUSSION

In this work, first, second and third natural frequencies of porous-FGB with three supporting types, C-C, S-S and C-F are calculated using ANSYS APDL and the element "SHELL281". In additional to the supporting types, the impacts of length/height ratio L/h, power-law index K, type of porosity distribution and porosity index α are investigated.

5.1 Even porous-FGB

Figure 9 illustrates the natural frequency parameters results of even porous-FGB when the porosity index α increases from zero to 0.3 for various supporting type and power-law index K. For first mode, the frequency parameter reduces when the power-law index K rises at any porosity index and any supporting types (see Figure 9(a)). In other side, the impact of porosity index is differing and depending on power-law index. For example, the frequency parameter increases when the porosity index increases at K=0, while, for K=10, For any supporting type, the frequency parameter falls as the porosity index rises. In other hand, the frequency parameter of C-C beam is larger than that of S-S and C-F beams (see Figure 9(a)). The same behavior is found in second and third natural frequencies (see Figure 9(b) and (c)). Also, the value of frequency parameter increases with increasing the mode number.

To explain the above results, the frequency of Euler - Bernoulli beam is considered, as an example, and the general equation are written as [35]:

$$\omega_i = (\beta_i L)^2 * \sqrt[2]{\frac{E_{eq}*I}{\rho_{eq}*A*L^4}},\ i = mode\ number \qquad (6)$$

The $\beta_i L$ value depends on the supporting type, A and I are the cross-section area and second moment of area of beam and their values are constant in this work. The value of $\sqrt[2]{\frac{E_{eq}}{\rho_{eq}}}$ is the effective part in Eq. (6). This part $\sqrt[2]{\frac{E_{eq}}{\rho_{eq}}}$ depends on modulus ratio of FG beam $\frac{E_{bottom}}{E_{top}}$, density ratio of FG beam $\frac{\rho_{bottom}}{\rho_{top}}$, power-law index and porosity index. In this work, the modulus and density ratio are constant and smaller than 1 as illustrated in Table 1: modulus ratio= $\frac{70}{380}$ and density ratio= $\frac{2707}{3960}$. According Eq. (1), when K=0 and infinity the equivalent material properties are the material properties of metal and ceramic respectively. When the power-law increases (larger than zero) the equivalent material will be larger than the metal material properties and smaller than the ceramic material properties. According to modulus and density ratio: modulus ratio=$\frac{70}{380}$ and density ratio=$\frac{2707}{3960}$, the equivalent modulus increases with rate larger than that of equivalent density for the same power-law index, therefor, the part $\sqrt[2]{\frac{E_{eq}}{\rho_{eq}}}$ increases with increasing power-law index and this leads to increases frequency.

In order to investigate the impact of porosity index, the porosity in porous-FGB is assumed to effect averagely on the material properties [1]. This means the porosity is found in metal and ceramic materials at the same time and the impact of porosity depends on porosity index and function of porosity distribution in additional to average of the modulus and density of metal and ceramic (see Eq. (2)). In even porous-FGB, the function of porosity distribution is constant and don't depend on the position in height of beam, i.e., z direction. Generally, the porosity existence causes reduction in material properties elastic modulus and density. For pure metal beam, the reducing rate of modulus due to porosity is larger than the reducing rate of density, therefore, the part $\sqrt[2]{\frac{E}{\rho}}$ reduces and this leads to increase the frequency of pure beam. But for pure metal beam, the reducing rate of modulus due to porosity is smaller than the reducing rate of density, therefore, the part $\sqrt[2]{\frac{E}{\rho}}$ reduces and this leads to decrease the frequency of pure beam. For porous-FGB, i.e., 0≤K≤∞, the increase of porosity index affects reversely on the frequency of beam while increase of the power-law index affects proportionally on the frequency of beam. In other words, the impact of power-law index is opposite to the impact of porosity index and the part $\sqrt[2]{\frac{E_{eq}}{\rho_{eq}}}$ depends on the combination effect of these two indices. Therefore, the part $\sqrt[2]{\frac{E_{eq}}{\rho_{eq}}}$ decreases at high porosity index and at any power-law index. It can see that the frequency decreases when the porosity index increases at high power-law index.

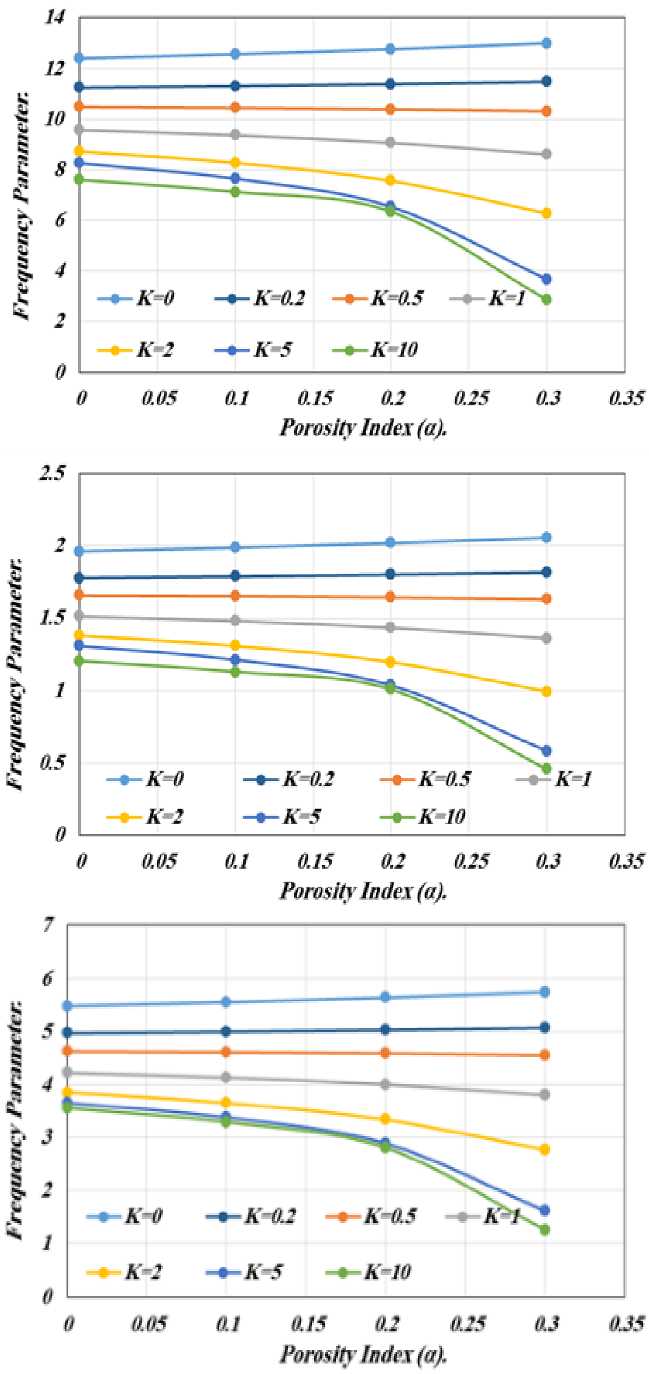

(a) 1st MODE

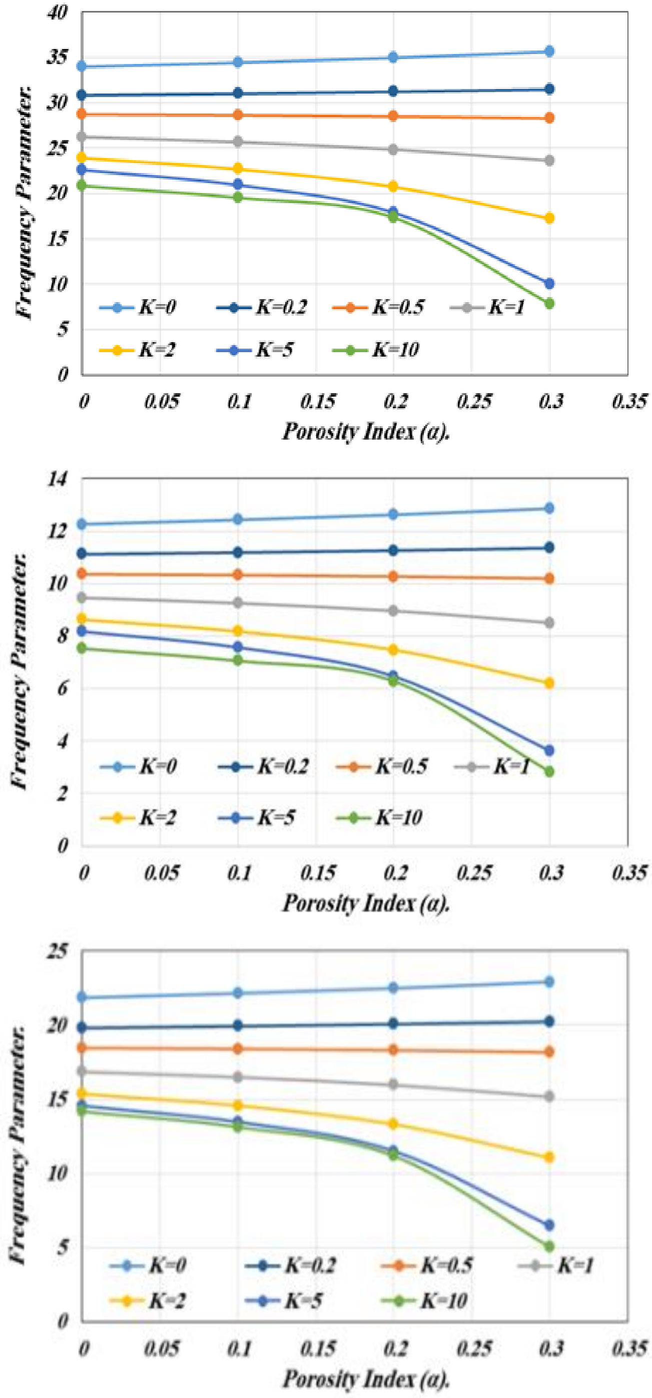

(b) 2nd MODE

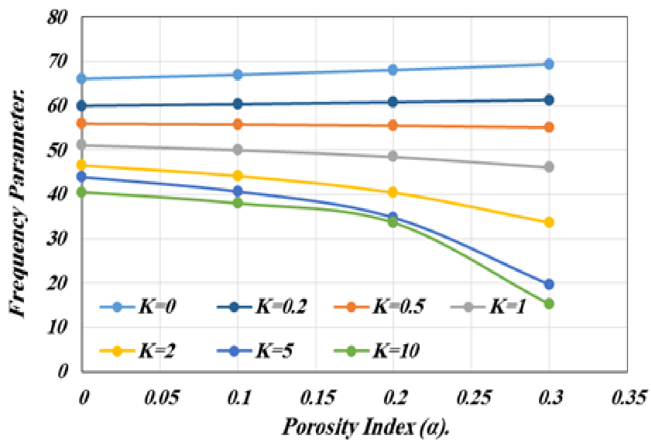

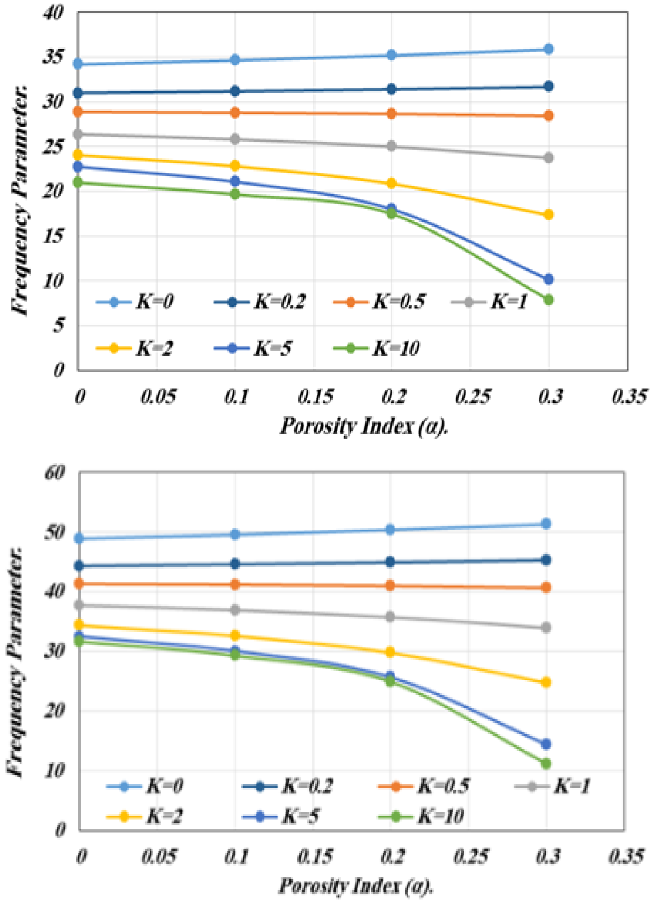

(c) 3rd MODE

Figure 9. The variation of the first, second and third frequency parameters of even porous-FGB due to variation of porosity index (α-index) for different supporting types when L/h=40

Figure 10 shows the natural frequency parameters results of even porous-FGB when the power-law index K increases from zero to 10 for different porosity index and supporting type. At every power-law index K, the frequency parameter falls as the porosity index rises and any supporting types. In other hand, the frequency parameter of C-C beam is larger than that of S-S and C-F beams (see Figure 10(a)). The same behavior is found in second and third natural frequencies (see Figures 10(b) and (c)). Also, the value of frequency parameter increases with increasing the mode number.

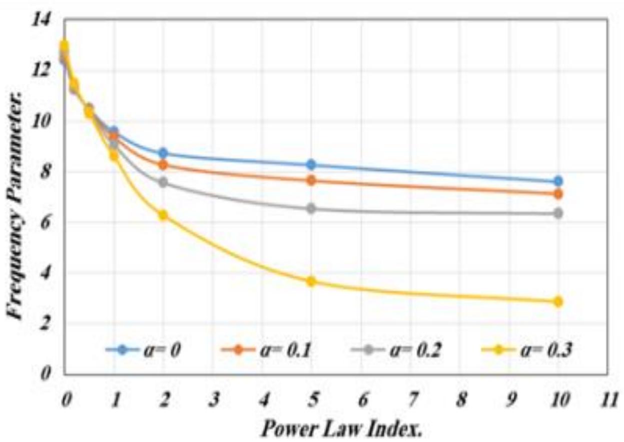

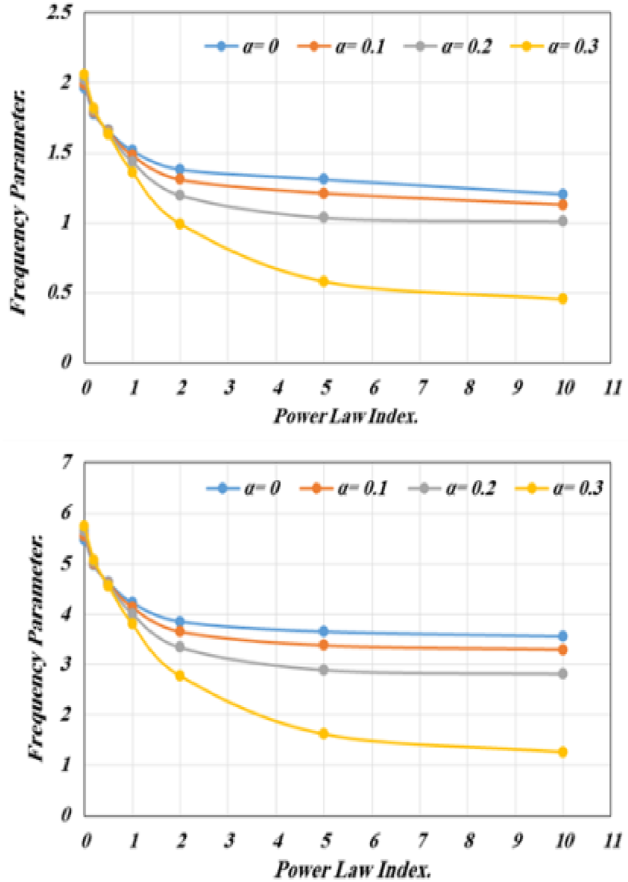

(a) 1st MODE

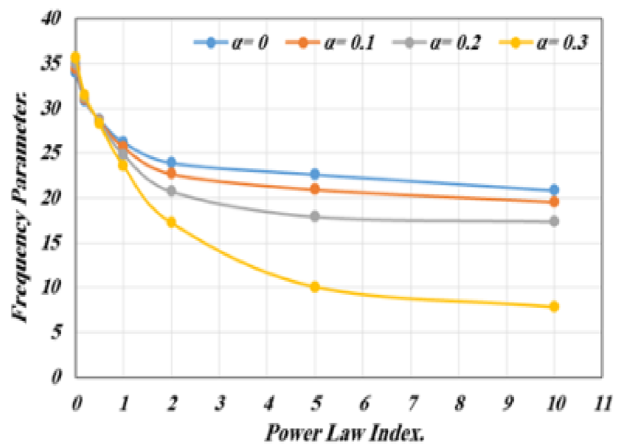

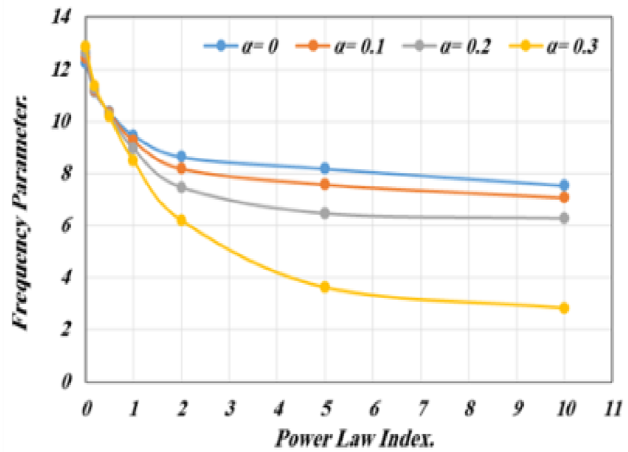

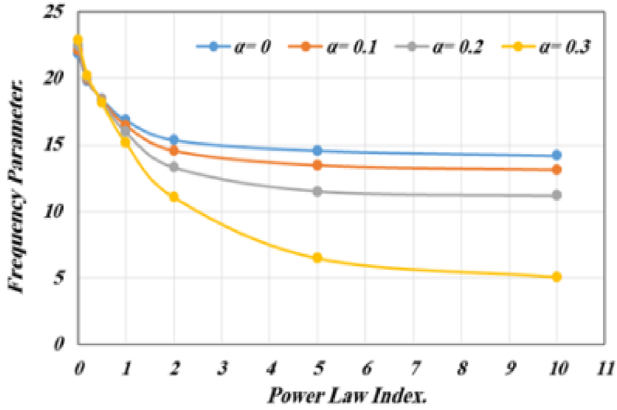

(b) 2nd MODE

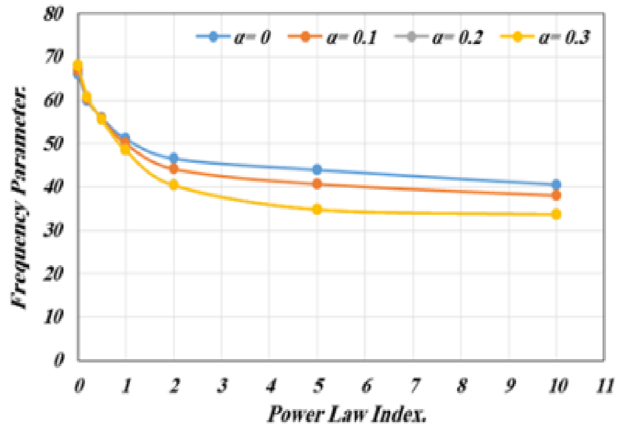

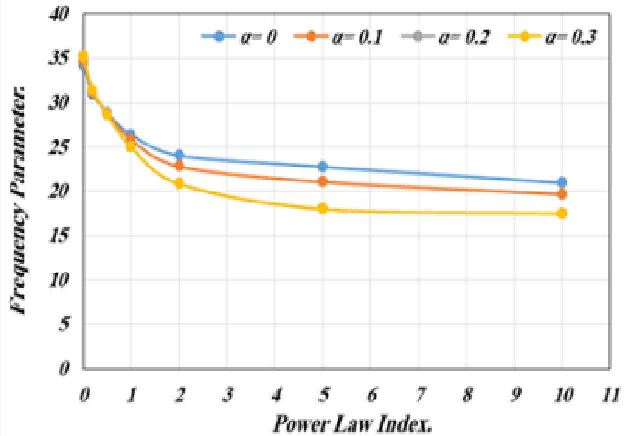

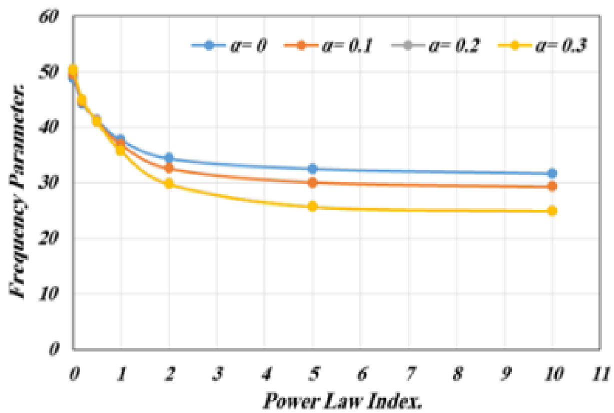

(c) 3rd MODE

Figure 10. The variation of the first, second and third parameters of even porous-FGB due to variation of power-law index K for different supporting types when L/h=40

5.2 Uneven-I porous-FGB

Figures 11 and 12 show the impacts of the porosity index and power-law index on the natural frequency parameters of porous-FGB for Uneven-I porosity distribution function and different supporting type. From Figure 11, the first frequency parameter reduces slightly when the porosity index rises at any power-law index and any supporting types (see Figure 11(a)). In other side, the influence of power-law index on the natural frequency parameters appears sharply and take the same profile in first, second and third natural frequency (see Figures 11(b) and (c)). Also, the value of frequency parameter increases with increasing the mode number. For Uneven-I porosity distribution function, the influence of porosity depends on z coordinate and concentrates at the center of FG beam. The influence of Uneven-I porosity distribution function is less than that of even one, therefore, the slight variation in natural frequency parameter is appear as shown in Figure 12.

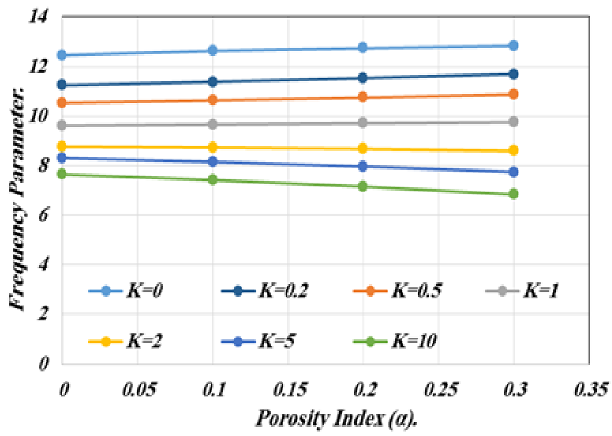

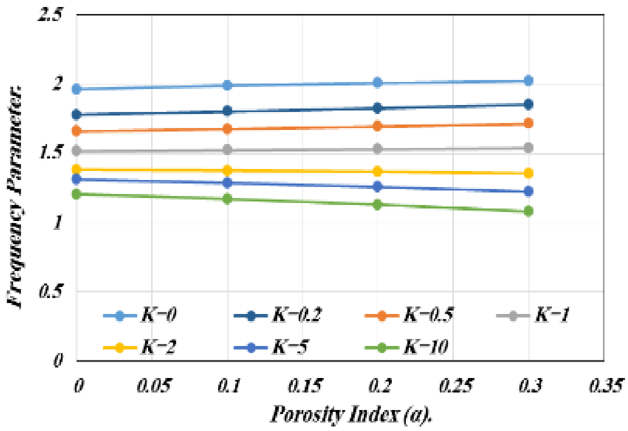

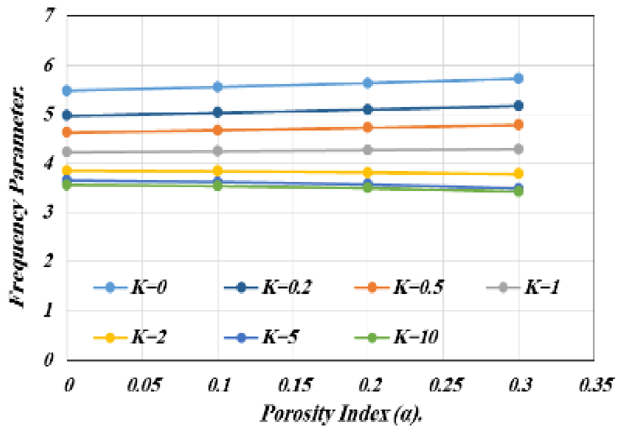

(a) 1st MODE

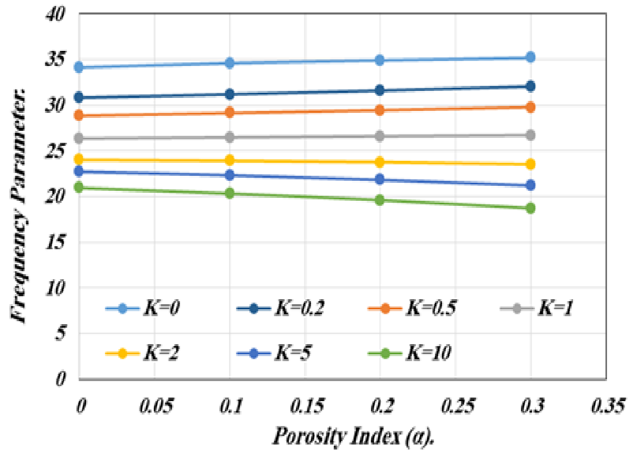

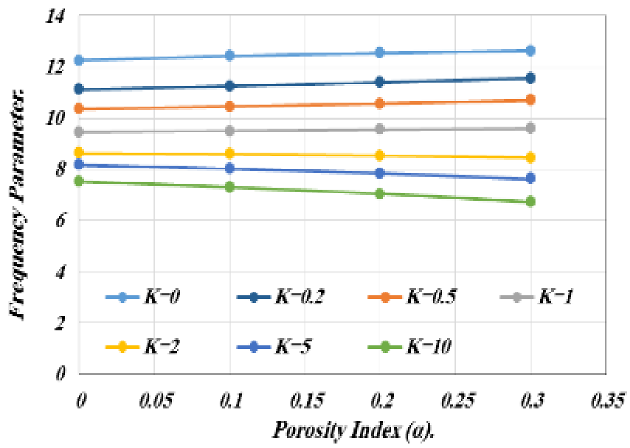

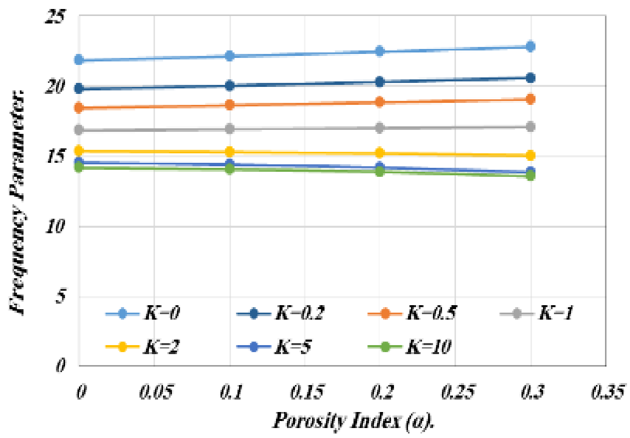

(b) 2nd MODE

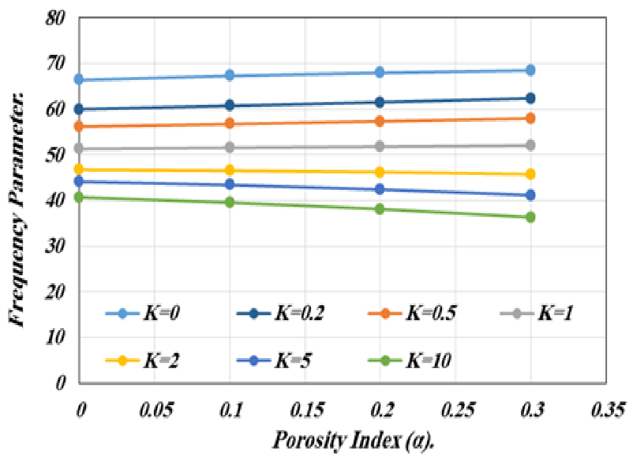

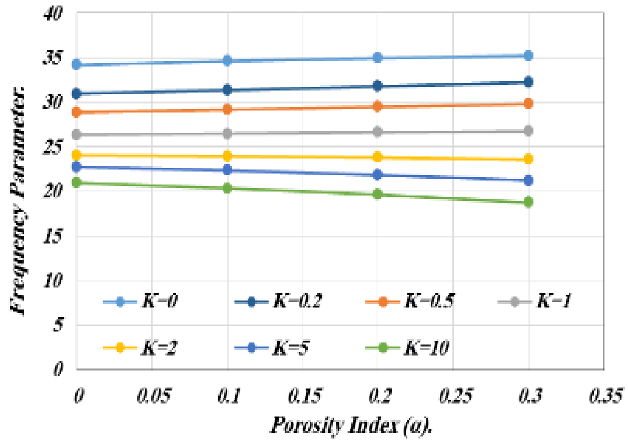

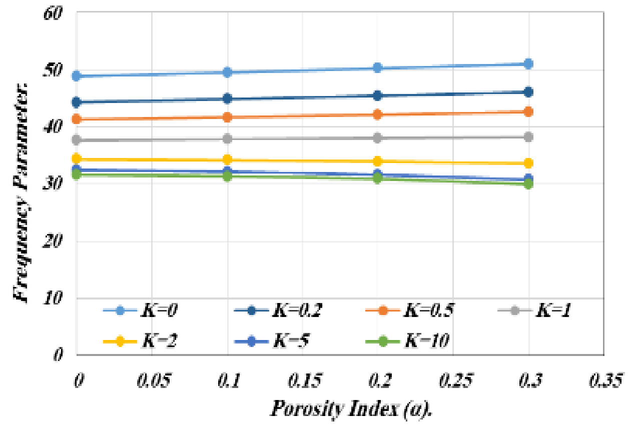

(c) 3rd MODE

Figure 11. The variation of the first, second and third frequency parameters of uneven-I porous-FGB due to variation of porosity index (α-index) for different supporting types when L/h=40

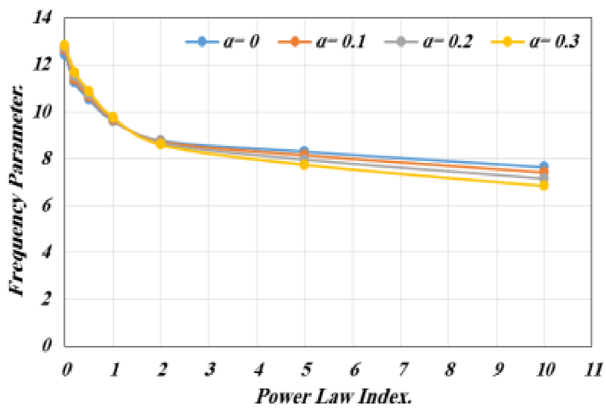

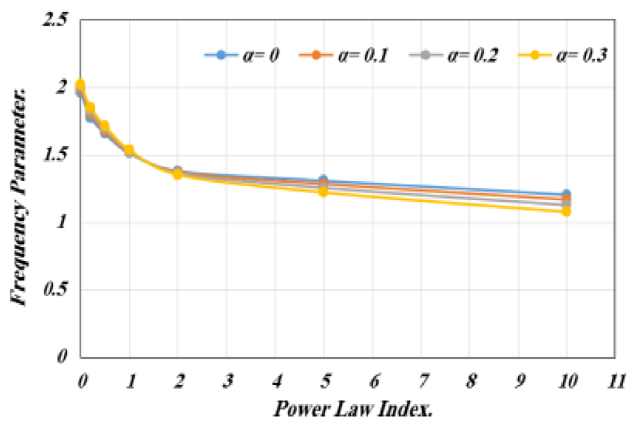

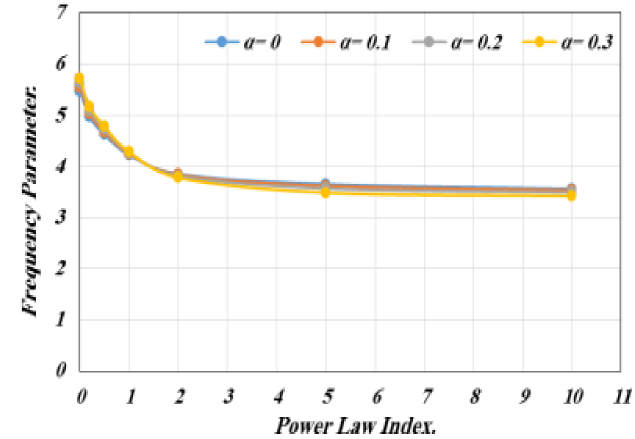

(a) 1st MODE

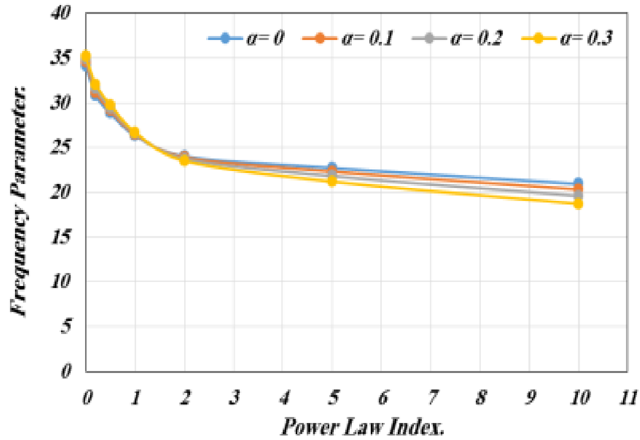

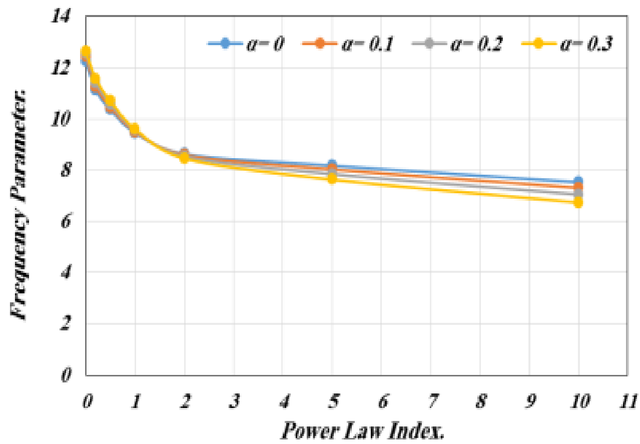

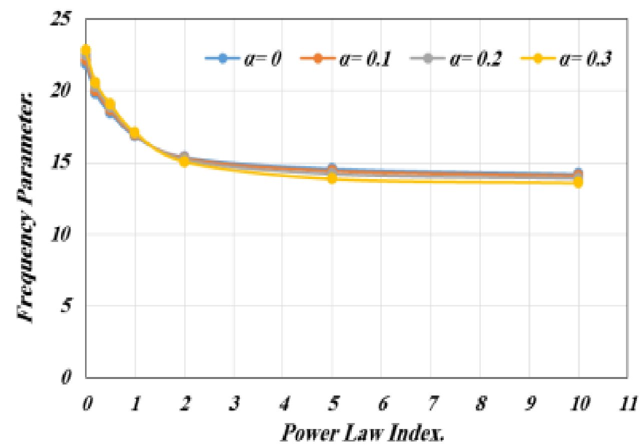

(b) 2nd MODE

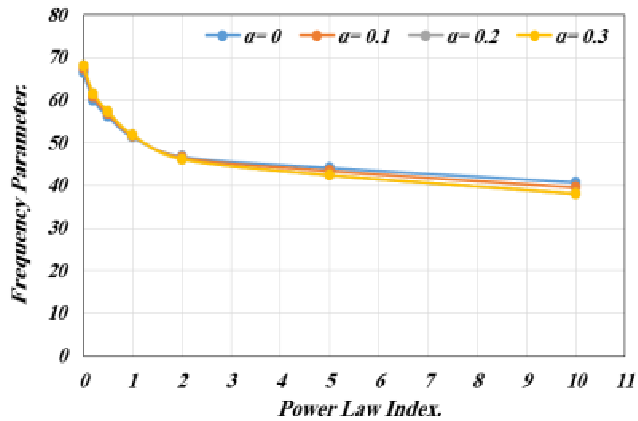

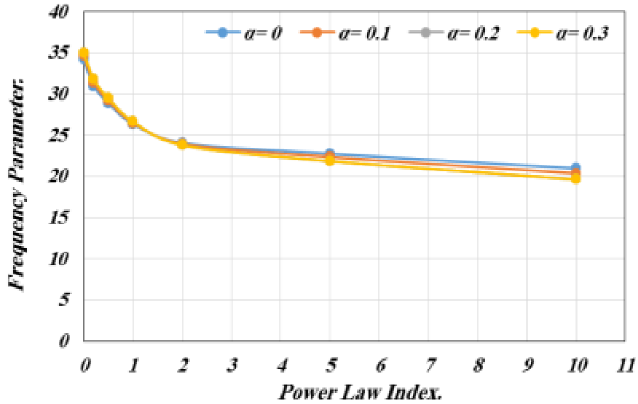

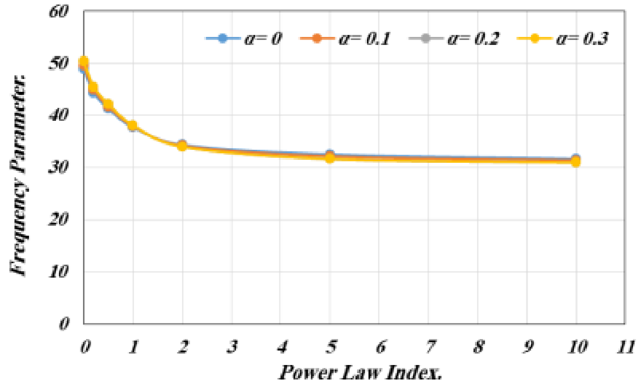

(c) 3rd MODE

Figure 12. The variation of the first, second and third frequency parameters of uneven-I porous-FGB due to variation of power-law index K for different supporting types when L/h=40

5.3 Uneven-II porous-FGB

Figures 13 and 14 show the impacts of the porosity index and power-law index on the natural frequency parameters of porous-FGB for uneven-II porosity distribution function and different supporting type. From Figure 13, the first frequency parameter decreases when the porosity index increases at any power-law index and any supporting types (see Figure 13(a)). In other side, the effect of power-law index on the natural frequency parameters appears sharply and take the same profile in first, second and third natural frequency (see Figures 13(b) and (c)). Also, the value of frequency parameter increases with increasing the mode number. For uneven-II porosity distribution function, the influence of porosity depends on z coordinate and concentrates at the edges of FG beam. The influence of uneven-II porosity distribution function is larger than that of Uneven-I porosity distribution function and smaller than that of even one. Therefore, Figure 14 shows sharply the variation in natural frequency parameter due to porosity distribution function, supporting type and mode number.

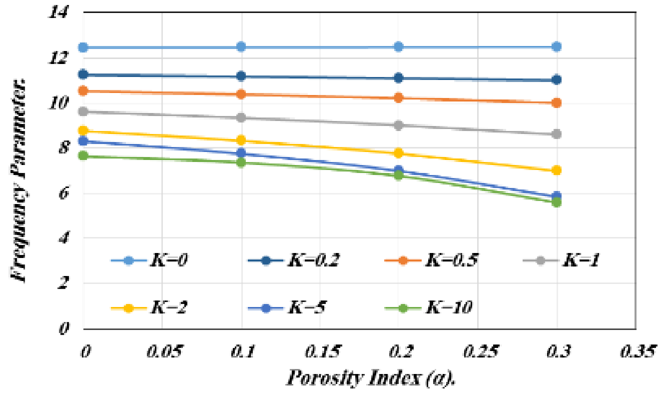

C-C

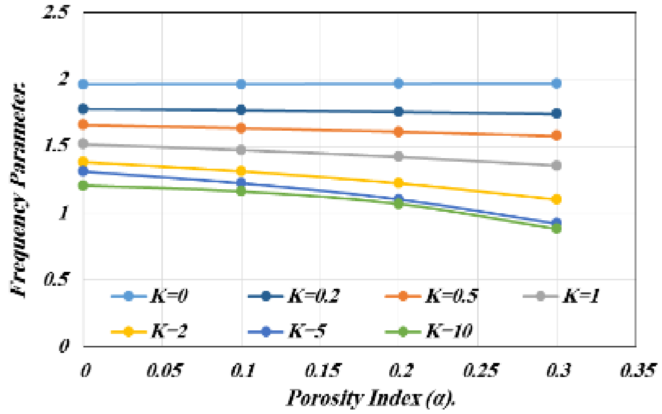

C-F

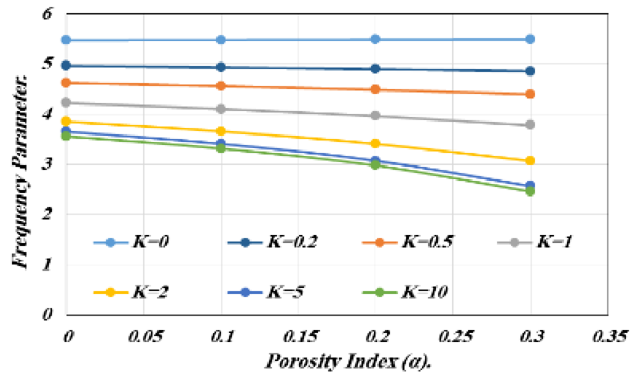

S-S

(a) 1st MODE

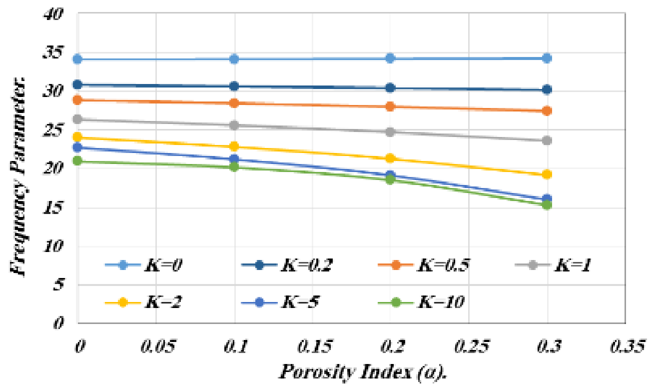

C-C

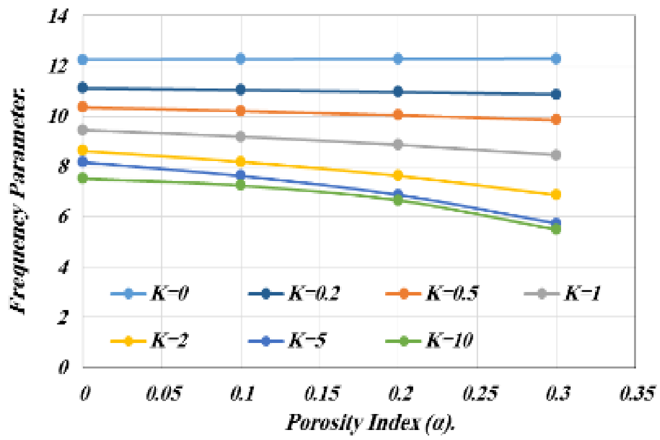

C-F

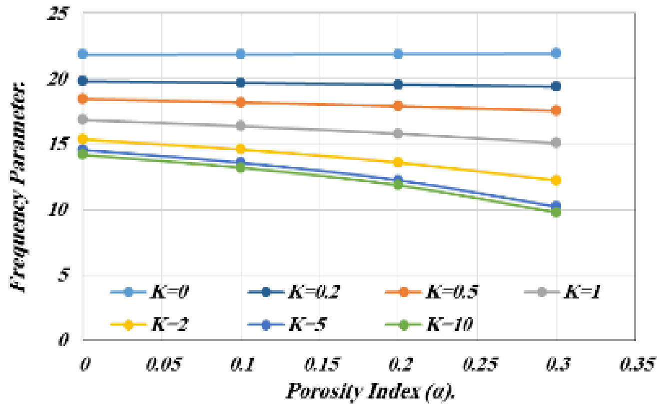

S-S

(b) 2nd MODE

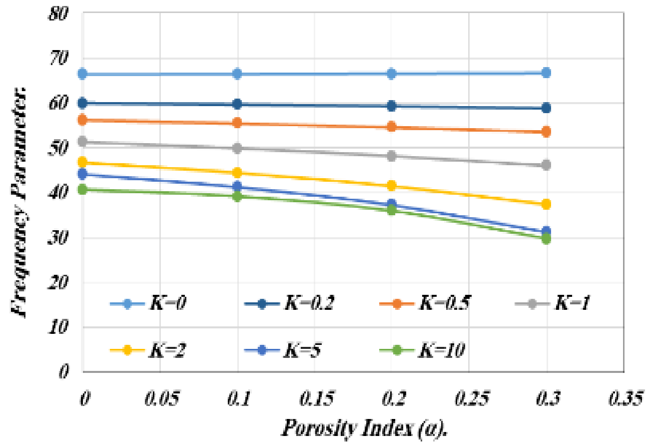

C-C

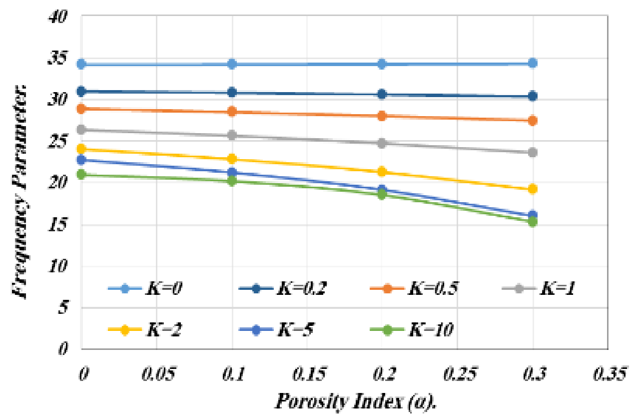

C-F

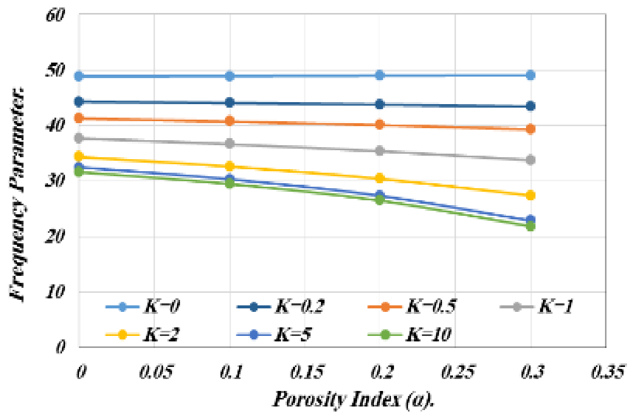

S-S
(c) 3rd MODE

Figure 13. The variation of first, second and third frequency parameters of uneven-II porous-FGB due to variation of porosity Index (α-index) for different supporting types when L/h=40

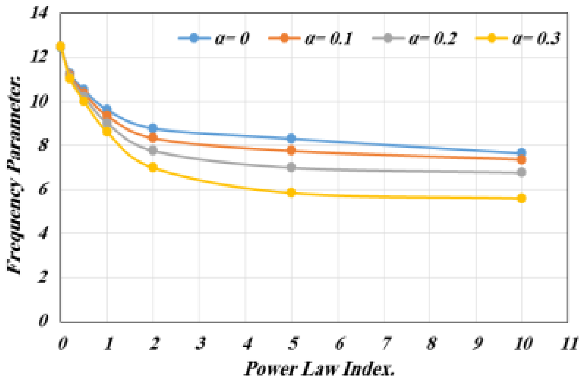

C-C

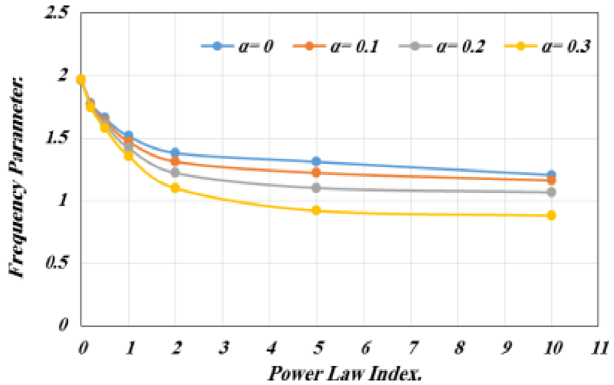

C-F

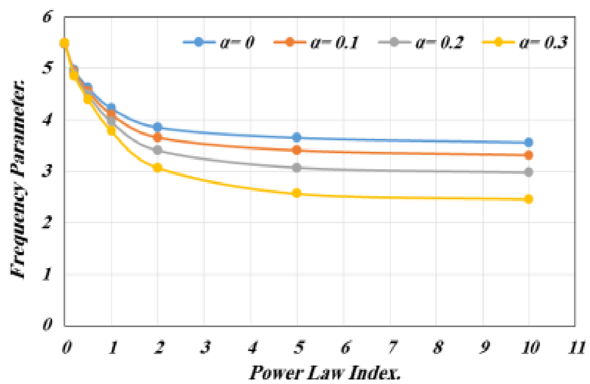

S-S
(a) 1st MODE

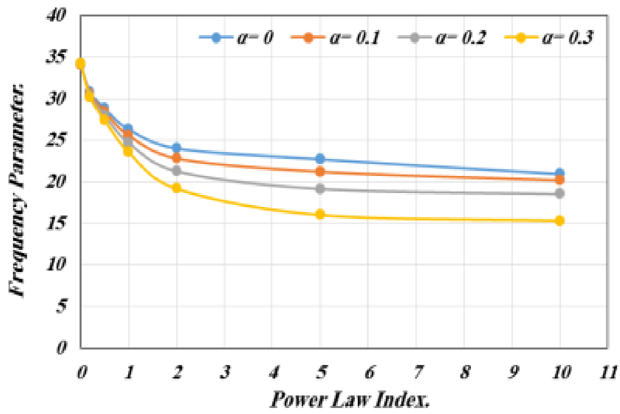

C-C

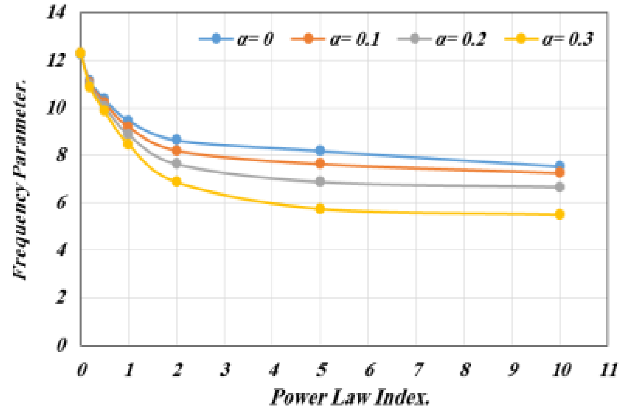

C-F

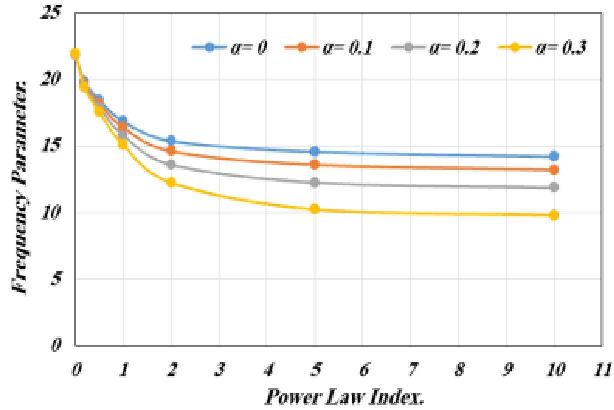

S-S
(b) 2nd MODE

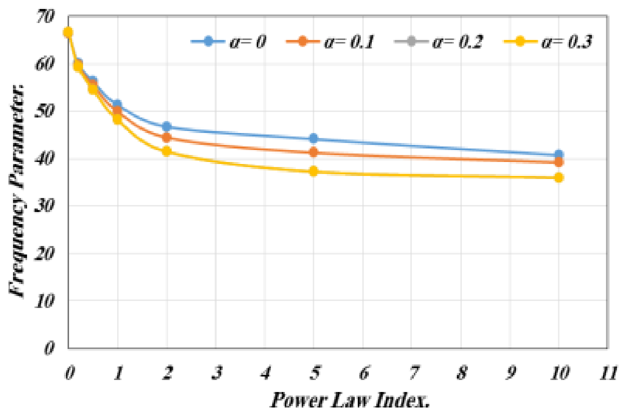

C-C

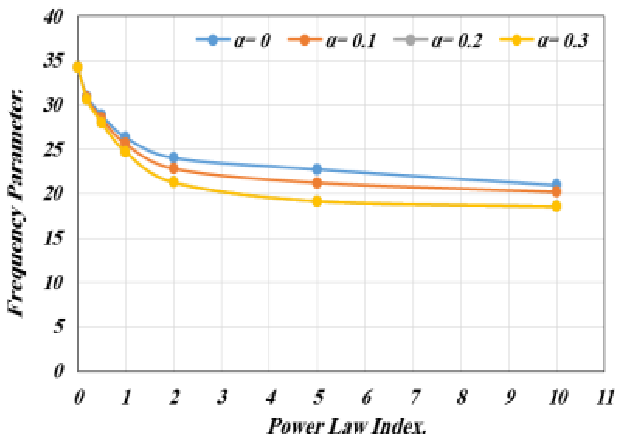

C-F

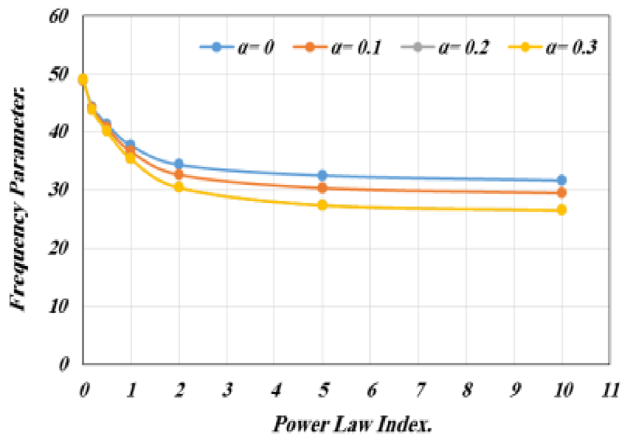

S-S

(c) 3rd MODE

Figure 14. The variation of the first, second and third frequency parameters of uneven-II porous-FGB due to variation of power-law index K for different supporting types when L/h=40

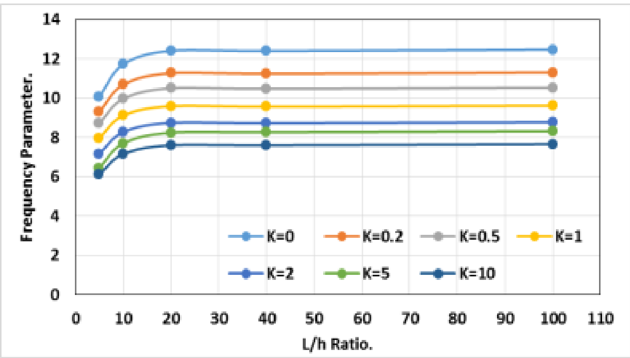

C-C

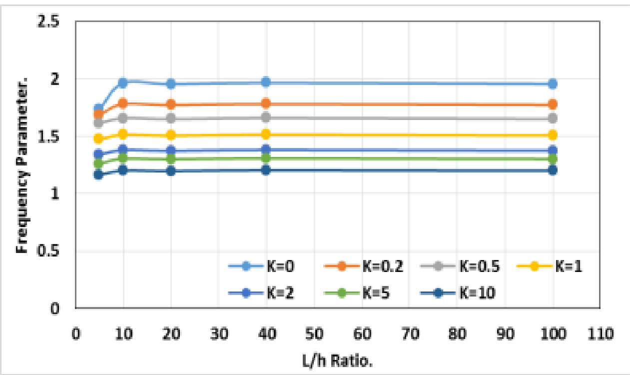

C-F

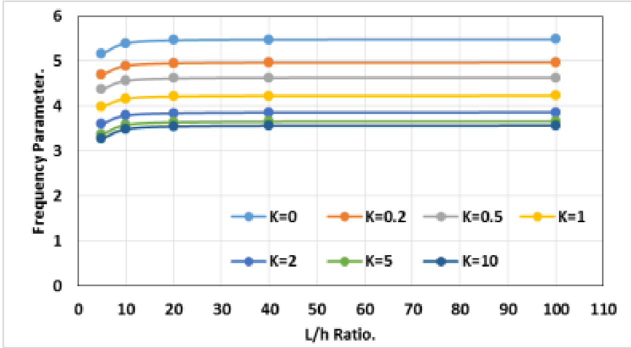

S-S

(a) α-index=0

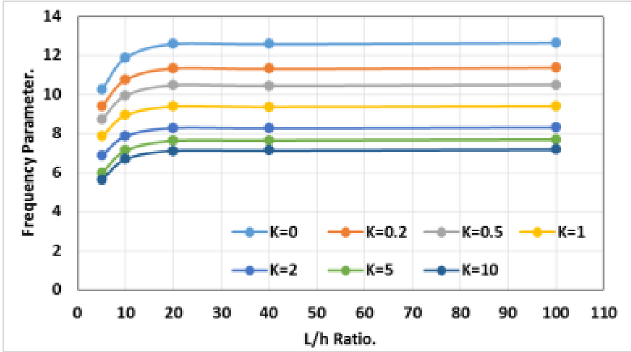

C-C

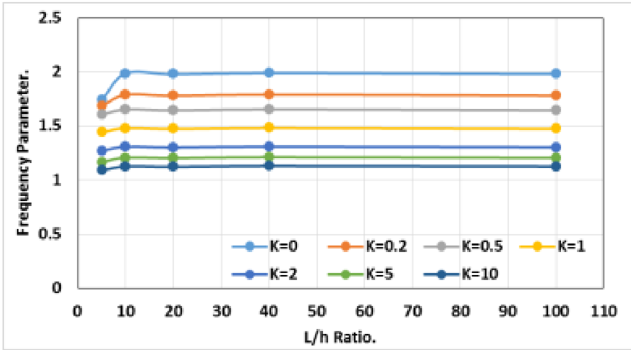

C-F

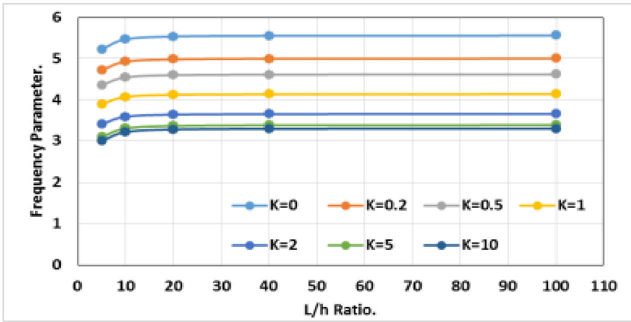

S-S

(b) α-index=0.1

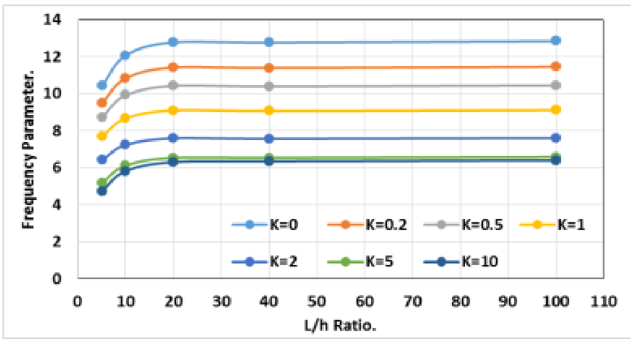

C-C

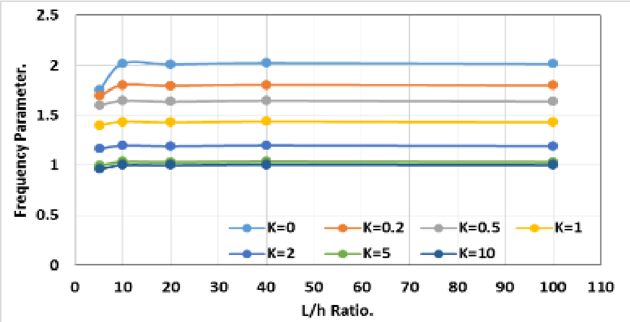

C-F

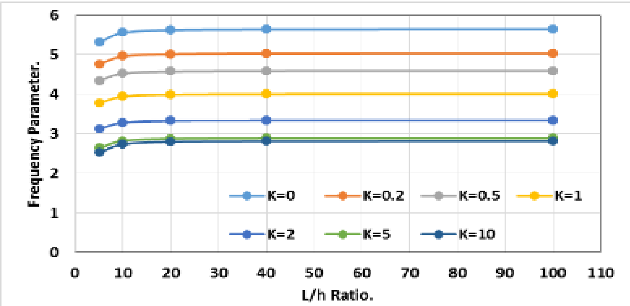

S-S

(c) α-index=0.2

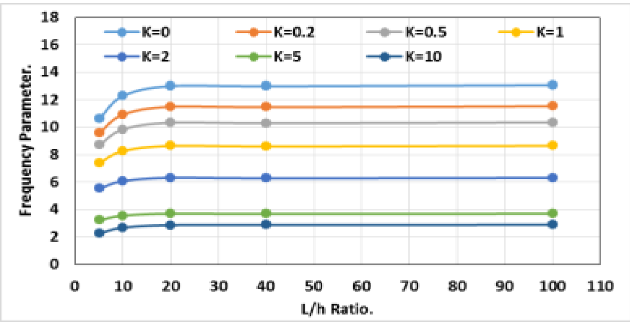

C-C

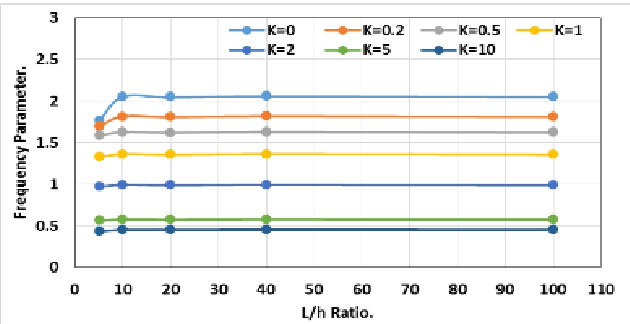

C-F

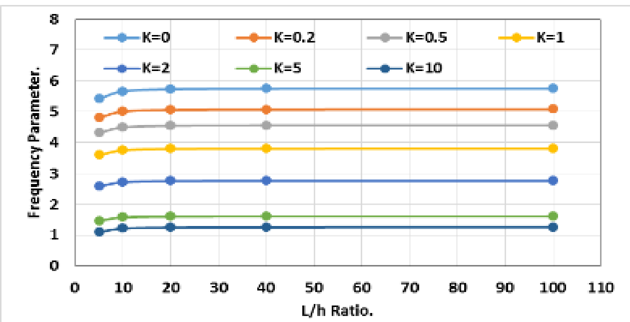

S-S

(d) α-index=0.3

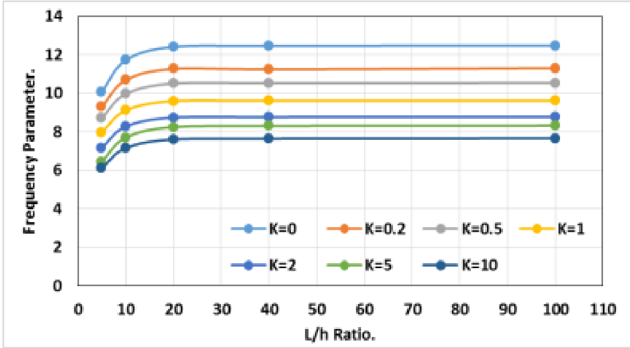

C-C

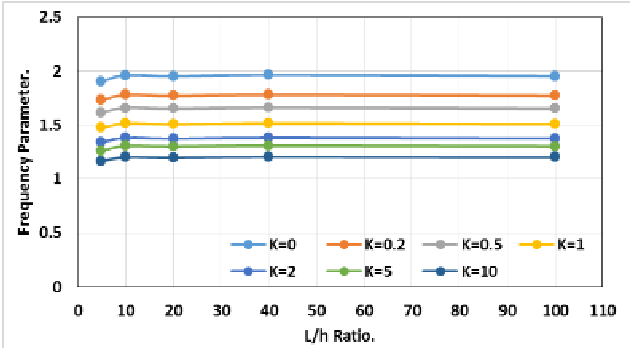

C-F

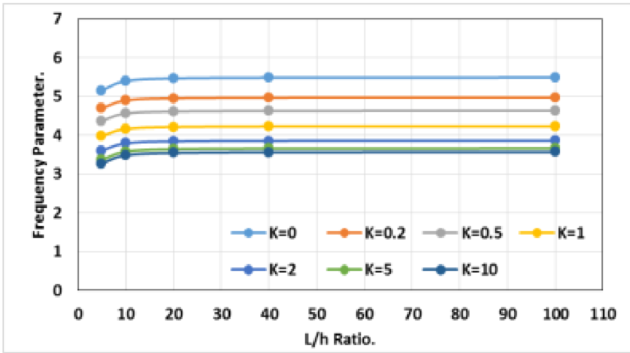

S-S

(a) α-index=0

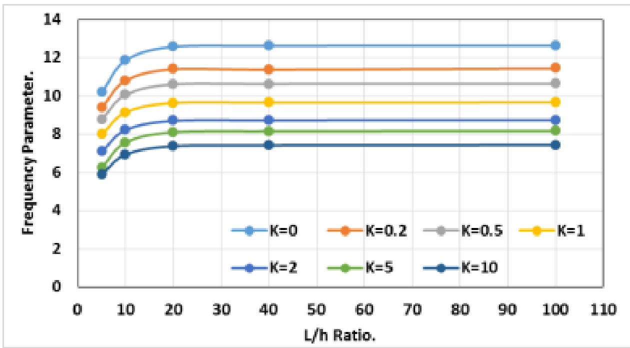

C-C

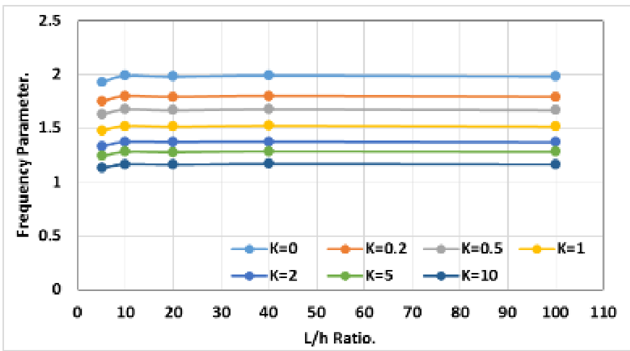

C-F

Figure 15. The impact of length-to height ratio on the first natural frequency parameter of the even porous-FGB under different supporting types for different power-law Index and different porosity index

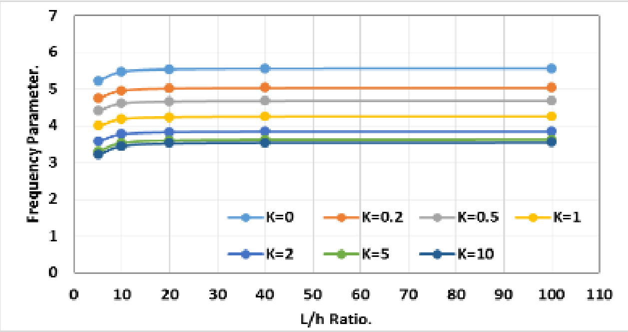

S-S

(b) α-index=0.1

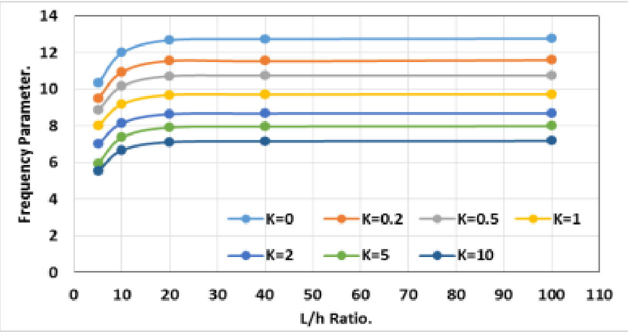

C-C

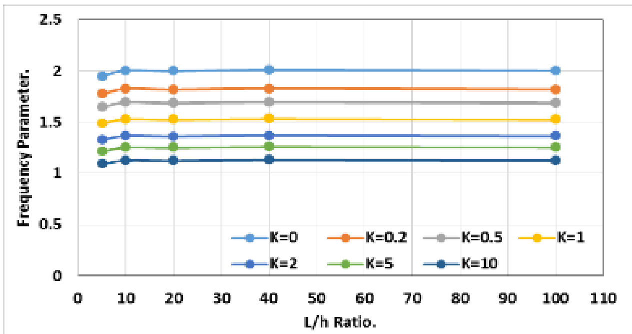

C-F

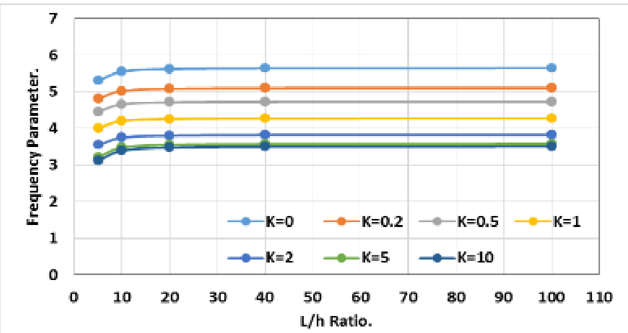

S-S

(c) α-index=0.2

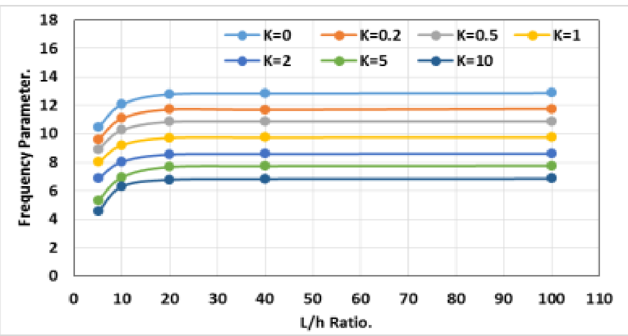

C-C

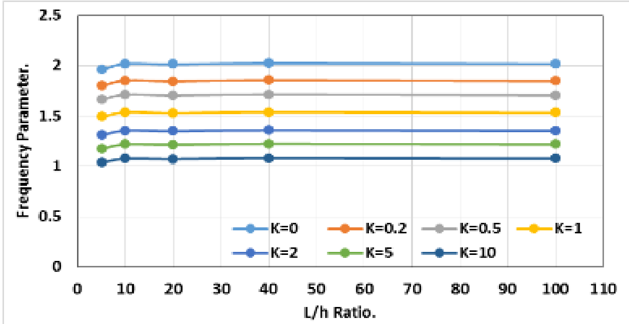

C-F

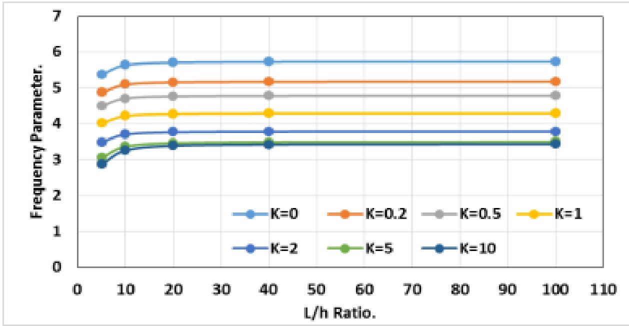

S-S

(d) α-index=0.3

Figure 16. The impact of length-to-height ratio on the first natural frequency parameter of the uneven-I porous-FGB under different supporting types for different power-law index and different porosity index

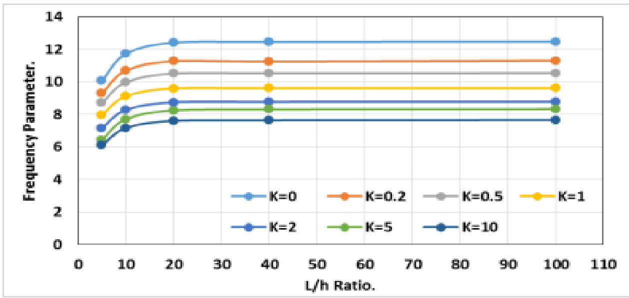

C-C

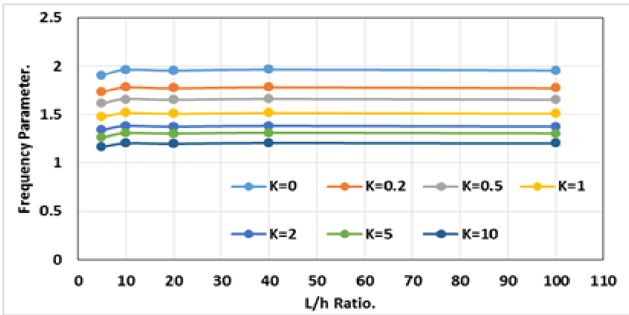

C-F

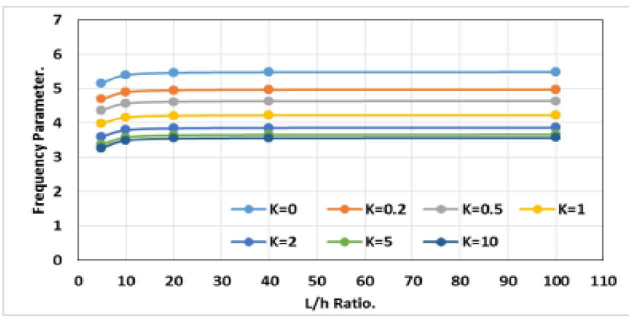

S-S

(a) α-index=0

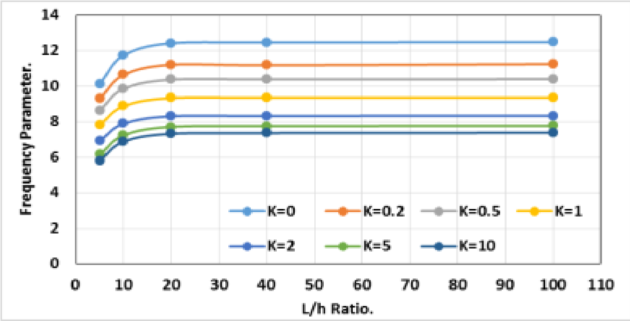

C-C

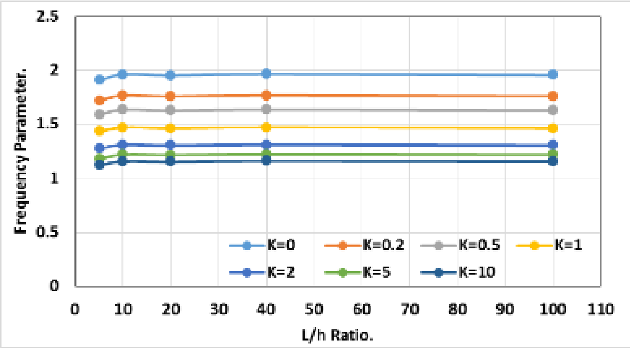

C-F

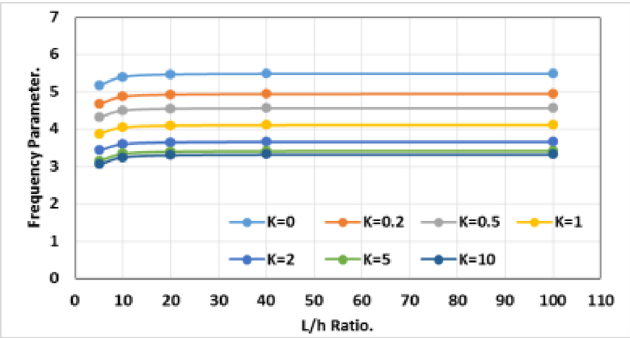

S-S

(b) α-index=0.1

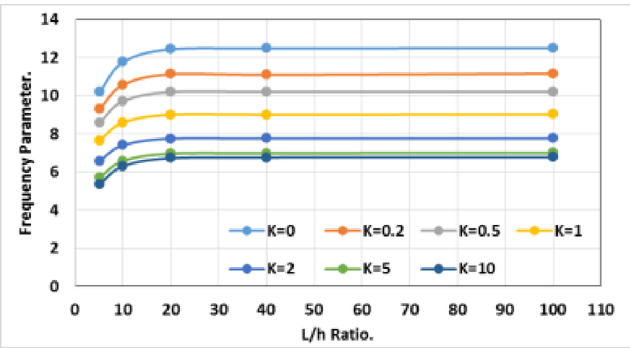

C-C

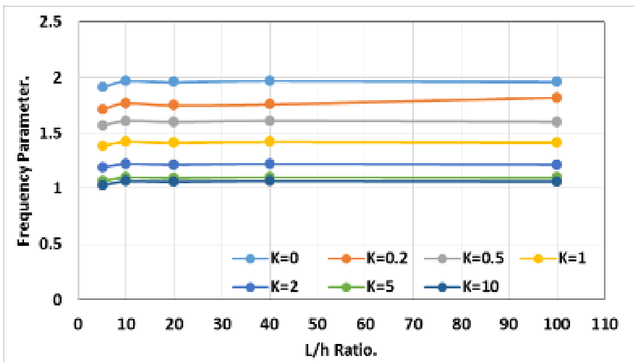

C-F

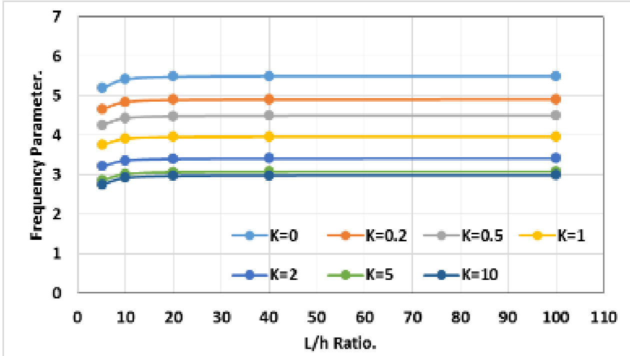

S-S

(c) α-index=0.2

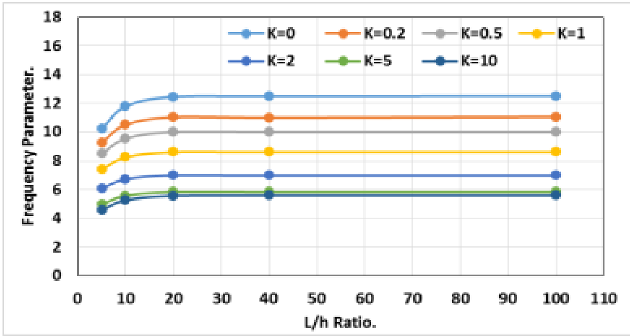

C-C

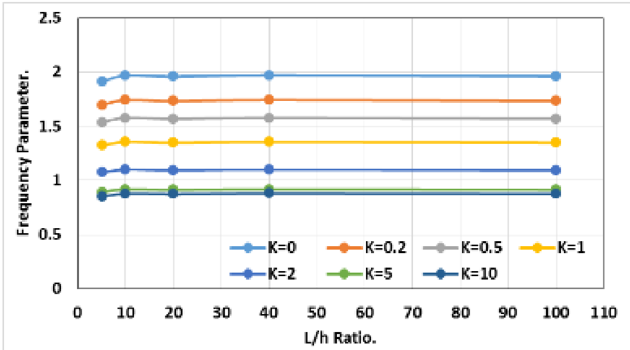

C-F

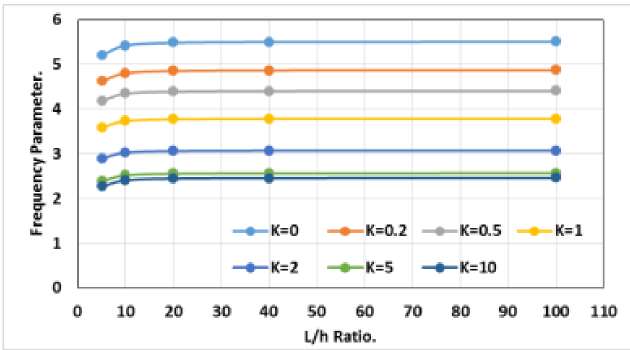

S-S

(d) α-index=0.3

Figure 17. The impact of length-to-height ratio on the first natural frequency parameter of the uneven-II porous-FGB under different supporting types for different power-law index and different porosity index

5.4 Effect of length/height ratio

The impact of length/height ratio on the first natural frequency parameter of porous, Even, Uneven-I and Uneven-II. FG beam under different supporting types for different power-law and porosity index are shown in Figures 15-17 respectively. Generally, the effect of length-to-height ratio on the first frequency parameter vanishes when the length-to-height ratio is greater than 20 for any supporting type, power-law index and porosity index. Also, the effect of length- to-height ratio on the first frequency parameter of C-C porous-FGB is greater than that of S-S and C-F porous-FGB respectively for any power-law index and porosity index. The reason of this behavior is similar to that described previously. The shear effect due to variation in material properties is small when the length-to-height ratio of porous-FGB increases, therefore the variation in the first frequency parameter decreases.

6. CONCLUSIONS AND FUTURE WORKS

In this work, the first, second and third natural frequencies of the porous-FGB are calculated by applying finite element method using ANSYS APDL software and element SHELL281. The first three natural frequencies are written as a frequency parameter to study the impacts of power-law index, porosity index, porosity distribution function, length/height ratio and supporting type. The combination of the impacts of theses parameters on the first three natural frequencies of the porous-FGB in additional to studying the influence of length/height ratio is the contribution of this work. The power-law index is assumed 0, 0.2, 0.5, 1, 2, 5 and 10, the porosity index is 0, 0.1, 0.2 and 0.3, the porosity distribution function is Even, Uneven-I and Uneven-II, the length/height ratio is 5, 10, 20, 40 and 100 and finally the supporting type is C-C, C-F and S-S beam. Based on earlier results, the following points can conclude:

(1) The comparison among the frequency results of the present new ANSYS model and that available in literatures shows an excellent agreement between them and proves the accuracy of the current ANSYS model.

(2) For even porous-FGB, the first three frequency parameters decrease when the power-law index K rises at any porosity index and any supporting types, while, the frequency parameter reduces when the porosity index rises for any power- law and any supporting types.

(3) For uneven-I porous-FGB, the first three frequency parameter decrease slightly when the porosity index rises at any power-law index and any supporting types. Also, the influence of power-law index on frequency parameters appear sharply and take the same profile in first, second and third natural frequency.

(4) For uneven-II porous-FGB, the first three frequency parameter decrease when the porosity index rises at any power-law index and any supporting types. In other side, the influence of power-law index on frequency parameters appears sharply and take the same profile in first, second and third natural frequency.

(5) The impact of the length/height ratio on the frequency parameters vanishes if the length/height ratio is equal or larger than 20.

(6) The values of frequency parameter increase with increasing the mode number for the same power-law index, porosity index, porosity distribution function, length/height ratio and supporting types.

(7) The uneven-I porosity function causes the smallest influence of porosity on the frequency parameters due to distribute the porosity near the center of cross section area of FGB.

The current research is the first step to analyze the dynamic response of the porous-FGB under different supporting conditions. In the future work, the harmonic and transient vibration behaviors are calculated by ANSYS APDL to investigate the impacts of power law index, porosity index, porosity function, length/height ratio and supporting type on the dynamic response.

REFERENCES

[1] Adıyaman, G. (2022). Free vibration analysis of a porous functionally graded beam using higher-order shear deformation theory. Journal of Structural Engineering & Applied Mechanics, 5(4): 277-288. https://doi.org/10.31462/jseam.2022.04277288

[2] Huang, C.Y., Chen, Y.L. (2016). Effect of mechanical properties on the ballistic resistance capability of Al_2O_3-ZrO_2 functionally graded materials. Ceramics International, 42(11): 12946-12955. https://doi.org/10.1016/j.ceramint.2016.05.067

[3] Naebe, M., Shirvanimoghaddam, K. (2016). Functionally graded materials: A review of fabrication and properties. Applied Materials Today, 5: 223-245. https://doi.org/10.1016/j.apmt.2016.10.001

[4] Udupa, G., Rao, S.S., Gangadharan, K.V. (2014). Functionally graded composite materials: An overview. Procedia Materials Science, 5: 1291-1299. https://doi.org/10.1016/j.mspro.2014.07.442

[5] Ton, L.H.T. (2022). Effect of porosity on free vibration of functionally graded porous beam based on simple beam theory. Technical Journal of Daukeyev University, 2(1): 1-10. https://doi.org/10.52542/tjdu.2.1.1-10

[6] Ton-That, H.L., Nguyen-Van, H., Chau-Dinh, T. (2021). A novel quadrilateral element for analysis of functionally graded porous plates/shells reinforced by graphene platelets. Archive of Applied Mechanics, 91: 2435-2466. https://doi.org/10.1007/s00419-021-01893-6

[7] Ton-That, H.L. (2020). A combined strain element to functionally graded structures in thermal environment. Acta Polytechnica, 60(6): 528-539 https://doi.org/10.14311/AP.2020.60.0528

[8] Parida, S.P., Jena, P.C., Dash, R.R. (2019). FGM beam analysis in dynamical and thermal surroundings using finite element method. Materials Today: Proceedings, 18: 3676-3682. https://doi.org/10.1016/j.matpr.2019.07.301

[9] Chen, Y., Jin, G., Zhang, C., Ye, T., Xue, Y. (2018). Thermal vibration of FGM beams with general boundary conditions using a higher-order shear deformation theory. Composites Part B: Engineering, 153: 376-386. https://doi.org/10.1016/j.compositesb.2018.08.111

[10] Ton-That, H.L., Nguyen-Van, H., Chau-Dinh, T. (2020). Static and buckling analyses of stiffened plate/shell structures using the quadrilateral element SQ4C. Comptes Rendus. Mécanique, 348(4): 285-305. https://doi.org/10.5802/crmeca.7

[11] Ebrahimi, F., Salari, E. (2015). Thermal buckling and free vibration analysis of size dependent Timoshenko FG nanobeams in thermal environments. Composite Structures, 128: 363-380. https://doi.org/10.1016/j.compstruct.2015.03.023

[12] Ton-That, H.L. (2020). The linear and nonlinear bending

analyses of functionally graded carbon nanotube-reinforced composite plates based on the novel four-node quadrilateral element. European Journal of Computational Mechanics, 29(1): 139-172 https://doi.org/10.13052/ejcm2642-2085.2915
[13] Ton-That, H.L., Nguyen-Van, H. (2021). A combined strain element in static, frequency and buckling analyses of laminated composite plates and shells. Periodica Polytechnica Civil Engineering, 65(1): 56-71. https://doi.org/10.3311/PPci.16809
[14] Chen, D., Yang, J., Kitipornchai, S. (2015). Elastic buckling and static bending of shear deformable functionally graded porous beam. Composite Structures, 133: 54-61. http://doi.org/10.1016/j.compstruct.2015.07.052
[15] Wattanasakulpong, N., Chaikittiratana, A. (2015). Flexural vibration of imperfect functionally graded beams based on Timoshenko beam theory: Chebyshev collocation method. Meccanica, 50: 1331-1342. https://doi.org/10.1007/s11012-014-0094-8
[16] Al Rjoub, Y.S., Hamad, A.G. (2017). Free vibration of functionally Euler-Bernoulli and Timoshenko graded porous beams using the transfer matrix method. KSCE Journal of Civil Engineering, 21: 792-806. https://doi.org/10.1007/s12205-016-0149-6
[17] Galeban, M.R., Mojahedin, A., Taghavi, Y., Jabbari, M. (2016). Free vibration of functionally graded thin beams made of saturated porous materials. Steel and Composite Structures, 21(5): 999-1016. http://doi.org/10.12989/scs.2016.21.5.999
[18] Fouda, N., El-Midany, T., Sadoun, A.M. (2017). Bending, buckling and vibration of a functionally graded porous beam using finite elements. Journal of Applied and Computational Mechanics, 3(4): 274-282. https://doi.org/10.22055/JACM.2017.21924.1121
[19] Akbaş, Ş.D. (2018). Forced vibration analysis of functionally graded porous deep beams. Composite Structures, 186: 293-302. https://doi.org/10.1016/j.compstruct.2017.12.013
[20] Amir, S., Soleimani-Javid, Z., Arshid, E. (2019). Size-dependent free vibration of sandwich micro beam with porous core subjected to thermal load based on SSDBT. ZAMM-Journal of Applied Mathematics and Mechanics/Zeitschrift für Angewandte Mathematik und Mechanik, 99(9): e201800334. https://doi.org/10.1002/zamm.201800334
[21] Zanoosi, A.A.P. (2020). Size-dependent thermo-mechanical free vibration analysis of functionally graded porous microbeams based on modified strain gradient theory. Journal of the Brazilian Society of Mechanical Sciences and Engineering, 42(5): 236. https://doi.org/10.1007/s40430-020-02340-3
[22] Zghal, S., Ataoui, D., Dammak, F. (2022). Static bending analysis of beams made of functionally graded porous materials. Mechanics Based Design of Structures and Machines, 50(3): 1012-1029. https://doi.org/10.1080/15397734.2020.1748053
[23] Rahmani, F., Kamgar, R., Rahgozar, R. (2020). Finite element analysis of functionally graded beams using different beam theories. Civil Engineering Journal, 6(11): 2086-2102. http://doi.org/10.28991/cej-2020-03091604
[24] Karamanli, A., Vo, T.P. (2021). A quasi-3D theory for functionally graded porous microbeams based on the modified strain gradient theory. Composite Structures, 257: 113066. https://doi.org/10.1016/j.compstruct.2020.113066
[25] Rahmani, M. (2021). Temperature-dependent vibration analysis of clamped-free sandwich beams with porous FG core. Journal of Modern Processes in Manufacturing and Production, 10(4): 61-77. https://doi.org/20.1001.1.27170314.2021.10.4.5.0
[26] Anirudh, B., Ganapathi, M., Anant, C., Polit, O. (2021). A comprehensive analysis of porous graphene-reinforced curved beams by finite element approach using higher-order structural theory: Bending, vibration and buckling. Composite Structures, 222: 110899. https://doi.org/10.1016/j.compstruct.2019.110899
[27] Nguyen, N.D., Nguyen, T.N., Nguyen, T.K., Vo, T.P. (2022). A new two-variable shear deformation theory for bending, free vibration and buckling analysis of functionally graded porous beams. Composite Structures, 282: 115095. https://doi.org/10.1016/j.compstruct.2021.115095
[28] Turan, M., Uzun Yaylacı, E., Yaylacı, M. (2023). Free vibration and buckling of functionally graded porous beams using analytical, finite element, and artificial neural network methods. Archive of Applied Mechanics, 93(4): 1351-1372. https://doi.org/10.1007/s00419-022-02332-w
[29] Neamah, R.A., Nassar, A.A., Alansari, L.S. (2022). Modeling and analyzing the free vibration of simply supported functionally graded beam. Journal of Aerospace Technology and Management, 14: e1522. https://www.jatm.com.br/jatm/article/view/1264/938.
[30] Marzoq, Z.A., Al-Ansari, L.S. (2021). Calculating the fundamental frequency of power law functionally graded beam using ANSYS software. IOP Conference Series: Materials Science and Engineering, 1090(1): 012014. https://doi.org/10.1088/1757-899X/1090/1/012014
[31] Help of ANSYS APDL Software Version 17.2.
[32] Kahya, V., Turan, M. (2017). Finite element model for vibration and buckling of functionally graded beams based on the first-order shear deformation theory. Composites Part B: Engineering, 109: 108-115. https://doi.org/10.1016/ j. compositesb.2016.10.039
[33] Nguyen, T.K., Nguyen, T.T.P., Vo, T.P., Thai, H.T. (2015). Vibration and buckling analysis of functionally graded sandwich beams by a new higher-order shear deformation theory. Composites Part B: Engineering, 76: 273-285. https://doi.org/10.1016/j.compositesb.2015.02.032
[34] Vo, T.P., Thai, H.T., Nguyen, T.K., Maheri, A., Lee, J. (2014). Finite element model for vibration and buckling of functionally graded sandwich beams based on a refined shear deformation theory. Engineering Structures, 64: 12-22. https://doi.org/10.1016/j.engstruct.2014.01.029
[35] Jebur, M.A., Alansari, L.S. (2023). Free vibration analysis of non-prismatic beam under clamped and simply supported boundary conditions. Mathematical Modelling of Engineering Problems, 10(5): 1630-1642. https://doi.org/10.18280/mmep.100513